THE UNIVERSITY OF MICHIGAN

COLLEGE OF ENGINEERING
Department of Mechanical Engineering
Heat Transfer and Thermodynamics Laboratory

Progress Report No. 4

(For the Period December 1961—July 1962)

PRESSURIZATION OF LIQUID OXYGEN CONTAINERS

J. A. Clark
H. Merte, Jr.
V. S. Arpaci
P. S. Larsen
P. Fennema
J. Beukema
H. C. Totten
B. Bailey
W. J. Yang
D. Rop

ORA Project 04268

under contract with:

NATIONAL AERONAUTICS AND SPACE ADMINISTRATION
GEORGE C. MARSHALL SPACE FLIGHT CENTER
CONTRACT NO. NAS-8-825
HUNTSVILLE, ALABAMA

administered through:

OFFICE OF RESEARCH ADMINISTRATION ANN ARBOR

July 1962

ensm

UMR 1254

v. 4

TABLE OF CONTENTS

TABLE OF CONTENTS (Concluded)

LIST OF FIGURES

Figure

Figure

Figure

NOMENCLATURE

A_I	area of interface = area of cross-section of tank (ft^2)
A_w	area of wall exposed to initial ullage space (ft^2)
$(C_p\mu/k)f$	Prandtl number at T_f
g	acceleration due to gravity
H_m	total enthalpy of mass entering ullage space during pressurization
h_{ga}	specific enthalpy at $T_g(\theta_p)$ and Pa (Btu/lbm)
$h_{g\theta_o}$	specific enthalpy at $T_g(\theta_o)$ and Pd (Btu/lbm)
h_m	specific enthalpy at T_{gi} and Pd (Btu/lbm)
$\bar{h}_g$	heat-transfer coefficient between pressurant gas and container wall (Btu/hr-ft^2-°F)
$\bar{h}_{gI}$	inside convective heat-transfer coefficient during hold time between liquid interface and gas space (Btu/hr-ft^2-°R)
$\bar{h}_{gv}$	inside convective heat-transfer coefficient during venting (Btu/hr-ft^2-°R)
$\bar{h}_{gw}$	inside convective heat-transfer coefficient during hold time between wall and gas space (Btu/hr-ft^2-°R)
$\bar{h}_o$	heat-transfer coefficient between container and ambient (Btu/hr-ft^2-°F)
$\bar{h}_{ot}$	outside convective heat-transfer coefficient from top of tank in forced convection
k_f	thermal conductivity of gas at film temperature T_f (Btu/hr-ft-°F)
Pa	14.7 psi
Pd	discharge pressure (lbf/$in.^2$)

Q	heat transfer from ullage space during hold time (Btu); $Q = q\Delta\Theta$ where $\Delta\Theta = \lvert\Theta_p - \Theta_o\rvert$, q = heat transfer rate (Btu/hr)
R	gas constant
T_f	film temperature at which properties for $\bar{h}_g$ are calculated [Eq. (8)]
T_{ga}	adiabatic mixed mean temperature
T_{gi}	actual initial pressurant temperature at inlet to tank
$T_g(\Theta_f)$	actual final pressurant temperature at inlet to tank
$T_g(\Theta_p)$	saturation temperature at one atmosphere
$T_g(\Theta_o)$	temperature of ullage after heat transfer during hold time $= \Theta_o - \Theta_p$
T_I	temperature of interface = saturation temperature at discharge pressure
T_{mf}	mean gas temperature in tank at end of run (data plot)
t_{wb}	temperature of wall at bottom of tank after discharge = saturation temperature at one atmosphere pressure
t_{wf}	arithmetic average, final wall temperature
t_{wt}	average temperature of wall at top of tank during venting
U_a	total internal energy of ullage gas at one atmosphere, pressure saturation conditions (Btu)
$U_{g\Theta_o}$	total internal energy of ullage gas at beginning of discharge (Btu)
V	volume of ullage space
Z_a	compressibility factor at Pa and $T_g(\Theta_p)$
$Z_{g\Theta_o}$	compressibility factor at Pd and $T_g(\Theta_o)$
β_f	compressibility of gas $= 1/T_f$

Δt	temperature potential (°F)
θ_f	end of discharge
θ_o	beginning of discharge
θ_p	time at pressurization
μ_f	viscosity of gas (lbm/ft-hr) at T_f
ρ_f	density of gas at film temperature T_f (lbm/ft^3)

ABSTRACT

Additional experimental data of final mean gas density are presented for inlet-gas temperatures up to approximately 600°F. Reduction of a portion of the Saturn data has been completed, with an analytical procedure used for computing the final mean temperature. These are compared with experimental measurements.

The results of a modified integral method are compared with the exact analytical solution for the pressurized discharge process.

Modifications of the reduced-gravity test facility necessary for operation at fractional gravities are described. Results and an explanation of the digital computer program used for data reduction with the transient sphere calorimeter are described.

Tentative data are presented showing the effect of system acceleration up to $a/g = 18.3$ on boiling heat transfer to liquid nitrogen at values of heat flux between $q/A = 5{,}000$ Btu/hr-ft^2 and $q/A = 20{,}000$ Btu/hr-ft^2.

A summary is given of the lumped-system transient in response to the injection of a highly soluble gas. Experimental data for the injection of nitrogen into liquid oxygen and of helium into liquid hydrogen are discussed in the light of the previously developed theory and the new extension of a variable gas enthalpy flux.

An approximate analysis of the dynamic growth of a single, stationary, inert gas bubble in a volatile liquid indicates that nonradial liquid convection due to translatory bubble motion plays a significant role for the observed rapid mass transfer. Experimental apparatus for bubble dynamic studies is being constructed.

I. OPTIMIZATION OF PRESSURIZED DISCHARGE PROCESSES IN CRYOGENIC CONTAINERS

A. Experimental Program

1. ADDITIONAL DATA—FINAL MEAN DENSITY

During the past period, experimental values of final mean density were obtained for the range of pressurant temperatures from 500°R to 1000°R for the adiabatic case. This series of runs has been numbered 58 A through M. A composite curve of the 58 series and the earlier 56 series, as well as an adiabatic case with inlet temperature ranges of 250°R to 500°R, is shown in Fig. 1. The performance of the new system during this series of runs was generally very satisfactory. The system has proven to be quite versatile, and the desired condition of a step-inlet temperature response at the beginning of discharge has been closely approximated.

A discrepancy still exists between the temperature indicated by thermocouple 25 (see Fig. 1) and the essentially identical temperatures indicated by thermocouples 26, 27, and 28. The results of final mean density are plotted as functions of both the temperature indicated by thermocouple 25 and the three identical temperatures of thermocouples 26, 27, and 28. It can be seen that the difference in temperature is about 80°F at a temperature level of 1000°R and about 30°F at a level of 500°R. The reason for the difference in temperature is not known, but it is possible that the gas undergoes some circulation which brings it into contact with the surrounding cold insulation before it passes over thermocouple 25. Since thermocouples 26, 27, and 28 do indicate identical temperatures, it seems realistic to consider thermocouple 26 as indicating the pressurant inlet temperature. It should be noted that since the theoretical mean density curve is relatively flat in this high temperature region, both temperatures correlate well with the theory. It should also be noted that the discrepancy is less at lower temperatures, so that the data reported prior to runs 58, which were obtained with the old system (e.g., runs 52 to 56) can be considered reliable.

2. EXPERIMENTAL APPARATUS

A schematic wiring diagram of two typical thermocouple circuits which measure the container-wall and gas-space temperatures is shown in Fig. 2. Also shown are the complete control panel, on which are mounted the thermocouple knife switches and the timing synchronizer; and the inlet-gas thermocouple circuit, which is recorded on the Sanborn recorder. The synchronizer

is used prior to each run to record the first timing signal of the Sanborn recorder on the visicorder recorder. Once the initial reference mark is established on each instrument, their timing signals are recorded independently for the remainder of each run. The gas and wall thermocouples are all 24 ga. copper-constantan couples except for the inlet-gas thermocouples, which are 30 ga. copper-constantan.

A complete drawing of the piping, valves, and heating wires immediately preceding the container inlets is shown in Fig. 3. The thermocouples numbered 29 through 40 consist of 24 ga. iron-constantan. The purpose of these thermocouples is to indicate the temperature of the piping so that this temperature can be matched with that of the bleed gas by adjusting the electrical power input to the heating wires wrapped around the pipes. The signals from these thermocouples are not recorded but only monitored with a Brown millivoltmeter, calibrated to indicate °F. Also shown in Fig. 3 is the wiring diagram of the terminal strip between the four Variacs and the heating wire elements.

A Fischer-Porter model 10A1735F rotameter is used in the gas-flow circuit to enable pressurant flow rates during the bleed period to be matched with rates during the discharge period. The rotameter purchased indicates directly pounds mass per minute of nitrogen gas flowing at a temperature of 0°F and a pressure of 60 psia. For any other gases or flow conditions it is necessary to make specific gravity, pressure, and temperature corrections as given in Instruction Bulletin 10A9020 published by the Fischer and Porter Co.

A Rockwell Model 800 positive-displacement gas meter has been incorporated into the flow circuit to provide an additional measurement of the pressurant flow-rate. The meter has been modified by connecting a potentiometer to the indicating dial so that a continuous recording of gas flow can be obtained. The signal from the potentiometer is connected through a switch to the AC-DC preamplifier unit of the Sanborn, the same unit which records the liquid level. Since the Rockwell meter is a total-volume flow measuring device, it is necessary to record only the initial and final voltage level of the potentiometer, the difference being an indication of the total volume transferred. The Sanborn unit is used to indicate liquid level during the remainder of the test run. The Rockwell meter has been calibrated using the Fischer and Porter rotameter and is accurate to within 3%. This meter will permit a more direct determination of the residual gas mass.

3. FUTURE EXPERIMENTAL TEST RUNS

A number of ambient runs have been obtained and the data are presently being reduced. The inlet temperature range included ambient to 550°F. These data will be reported during the next period.

Preliminary investigations are currently in progress to determine the source of the differential mass which has been observed by other investigators.

This differential mass is defined as the mass of gas which is obtained if the sum of the initial ullage gas mass plus the gas mass introduced into the tank as pressurant is subtracted from the mass of gas in the tank at the end of discharge, commonly called the residual mass. The residual mass is to be obtained from the thermocouple temperature indications at the end of the run, as was formerly done for the adiabatic and ambient runs. The mass of pressurant introduced was measured using the Sanborn and the Rockwell meters described above. The initial ullage mass will be determined by using the liquid-level indicator, which will determine the initial ullage volume, and by measuring the temperature distribution throughout the initial ullage space with the floating thermocouples. Because the amount of differential mass is small, very precise measurements of gas pressure, temperature, and flow rate are necessary. Some difficulty had been encountered in attempting to eliminate the gas leaks in the system. For the experiments prior to this report period, these leaks were not significant, but for the differential mass investigation the leaks must be reduced as much as possible.

4. ANALYSIS OF SATURN DATA

a. Introduction

Experimental data for pressurized discharge of liquid oxygen from a large tank have been received from the George C. Marshall Space Flight Center for the purpose of reducing the data for an arbitrary pressurant inlet temperature. The data-reduction method described in an earlier Progress Report[1] is being used. The runs received are numbered 51-44 and 51-54 (non-slosh runs), and 95-20 and 95-23 (slosh runs). To date, runs 51-44 and 51-54 have been reduced, and calculations are presently in progress for runs 95-20 and 95-23. In the following sections the calculation procedure followed for runs 51-44 and 51-54 are outlined and the numerical results presented. Necessary assumptions are stated when made.

b. Calculation of Initial Inlet Temperature of Pressurant

The arbitrary-inlet temperature theory makes use of a series of straight-line ramps to approximate the actual inlet temperature curve during the discharge period. Application of the theory thus requires a knowledge of the variation of the inlet temperature, the inlet location being $x = 0$, which is the initial liquid level in the container. For runs 51-44 and 51-54, the actual inlet temperature (thermocouple T-30) is measured at a significant distance from level $X = 0$, so that an approximation to the time-temperature plot is necessary. For these runs, an idealized time-temperature curve is assumed, as shown in Fig. 4. To determine T_{ga}, the ullage space is considered an insulated container initially containing saturated vapor at one atmosphere pressure, with subsequent pressurization by the same gas at a temperature T_{gi}. The effect of heat transfer from the relatively warm gas to the cold walls

and liquid oxygen during the hold time before discharge begins is taken into account by a First Law analysis.

To determine the heat flow out of the ullage space during the hold time, it is necessary to determine a value for the convective heat-transfer coefficient between the wall and the gas and between the liquid interface and the gas. Since the wall heat-transfer coefficient is governed by a natural convective process, it is first necessary to determine the temperature of the wall. The heat capacity of the wall is greater than the heat capacity of the enclosed gas by a factor of 20; therefore the assumption is made that the wall temperature remains the same as it was during venting to the atmosphere prior to pressurization. A value for $\bar{h}_{gv}$ can be calculated by determining the boil-off rate during venting, using $\bar{h}_o$ = 3 Btu/hr-ft^2-°R calculated below and using Eq. (9-10b) of Ref. 2, and correcting for an L/D effect with Eq. (9-13d). The value for $\bar{h}_{gv}$ calculated is found to be 1.5 Btu/hr-ft^2-°R. For $\bar{h}_{ot}$, Eq. (6-68) of Ref. 3 is used, with the top of the tank considered a flat plate with air flowing over it at a velocity of 10 mph. The solution yields $\bar{h}_{ot}$ = 1 Btu/hr ft^2 °R. Since the tank is not protected from the ambient, the effect of a probable build-up of frost can also be included. Reference 4 lists a value of 5 Btu/hr-ft^2-°R for the conductance of a frost layer having air flowing over it at a velocity of 10 mph. Thus, t_{wt} is calculated to be -160°F = 300°R. This value is used for both runs, 51-44 and 51-54.

An approximate value for $\bar{h}_{gw}$ can now be determined using Eq. (7-4a) of Ref. 2; a value of 3.5 Btu/hr-ft^2-°R is obtained. Similarly, $\bar{h}_{gI}$ is calculated from Eq. (7-8b) of Ref. 2 to be 1.0 Btu/hr-ft^2-°R. Although these equations do not strictly apply to this specific configuration, it is felt that the order of magnitude obtained is reasonable.

The First Law of Thermodynamics is now applied to flow into a closed container.

$$Q + H_m = U_{g\Theta_o} - U_a \tag{1}$$

where Q can be expresses as

$$Q = q(\Delta\Theta) = \left\{\bar{h}_{gw}A_w\left[t_{wt} - \frac{T_{ga}+T_g(\Theta_o)}{2}\right] + \bar{h}_{gI}A_I\left[T_I - \frac{T_{ga}+T_g(\Theta_o)}{2}\right]\right\}\Delta\Theta \tag{2}$$

By introduction of the perfect gas law, Eq. (1) becomes:

$$\frac{P_d V}{Z_{g\Theta_o} R T_g(\Theta_o)}(h_{g\Theta_o} - h_{ln}) + \frac{P_a V}{Z_a R T_g(\Theta_p)}(h_{ln} - h_{ga}) + V(P_a - P_d) - Q = 0 \tag{3}$$

In this equation, the only unknown is $T_g(\Theta_o)$, as $\rho_{g\Theta_o}$ and $h_{g\Theta_o}$ are functions of $T_g(\Theta_o)$. It is necessary to solve this equation by trial and error. For run 51-44, $T_g(\Theta_o)$ is found to be approximately 300°R, and for run 51-54 $T_g(\Theta_o)$ = 260°R. A plot of the actual inlet temperature and the assumed ramp, as calculated above, versus time is shown in Figs. 5 and 6 for the runs 51-44 and 51-54 respectively. The actual inlet temperature curve was obtained from the data plots of the thermocouple numbered T-30 in the series 51 runs.

c. Calculation of Final Mean Density

It is necessary to calculate the variables s, δ and η, defined in Ref. 1 as:

$$s = \frac{\bar{h}_g P}{\rho C_p A} \frac{x}{v} \tag{4}$$

$$\delta = \frac{\bar{h}_g P}{\rho' C_p' A_o} (\Theta - \frac{x}{v}) \tag{5}$$

$$\eta = \frac{1}{1 + \frac{\bar{h}_o P_o}{\bar{h}_g P}} \tag{6}$$

The nomenclature is the same as that used in Ref. 1. To obtain values for these variables, values of $\bar{h}_o$ and $\bar{h}_g$ must be specified.

The heat transfer coefficent between the container and the ambient is affected both by forced convection due to the 10 mph wind velocity, and by natural convection due to the large temperature difference between the wall and the ambient. For forced convection, Eq. (9-3) of Ref. 3 applies:

$$N_u = C(Re)^n \tag{7}$$

By evaluating the fluid properties at the film temperature, and since V_∞ = 10 mph, $\bar{h}_o$ is calculated to be 3.5 Btu/hr-ft^2-°F. For natural convection, Fig. 7-4 of Ref. 3 applies; thus $\bar{h}_o$ = 2 Btu/hr-ft^2-°F. Since these are the same order of magnitude, a mean value of $\bar{h}_o$ = 3 Btu/hr ft^2 °F is used in the subsequent calculations.

Because of the transient nature of the discharge process, a value for $\bar{h}_g$ is very difficult to obtain. For the purposes of this analysis, an overall mean value is calculated with use of the standard equations for natural convection heat transfer. A value for $\bar{h}_g$ was also calculated with forced convection considered, but it was found that $\bar{h}_g$ due to forced convection is

negligible for the conditions of flow in these runs. Since the wall temperatures throughout the run were not recorded, fluid properties are evaluated at a film temperature defined as

$$T_f = \frac{T_{wf} + T_{mf}}{2} \tag{8}$$

where t_{wf} is determined by

$$t_{wf} = \frac{t_{wt} + t_{wb}}{2} \tag{9}$$

The value of T_{mf} is the average value obtained from a data plot of gas temperature versus distance in the tank at the end of discharge. The equation used to determine $\bar{h}_g$ is Eq. (7-4a) of Ref. 2:

$$\frac{\bar{h}_g L}{k_f} = 0.13 \left[\frac{L^3 \rho_f^3 g \beta_f \Delta t}{\mu_f^2} \left(\frac{c_p \mu}{k} \right)_f \right]^{1/3} \tag{10}$$

Note that it is not necessary to define a length L since it cancels from both sides of the above equation. For the term Δt, two extreme conditions, at the beginning of discharge and at the end of discharge, are considered. Thus

$$\Delta t_{min} = T_g(\Theta_o) - t_{wt} \tag{11}$$

and

$$\Delta t_{max} = T_{mf} - t_{wf} \tag{12}$$

Solution of Eq. (10) for runs 51-44 and 51-54 results in

$$\bar{h}_{g\ max} = 4.5 \text{ Btu/hr-ft}^2\text{-°F}$$

$$\bar{h}_{g\ min} = 3.1 \text{ Btu/hr-ft}^2\text{-°F}$$

Since the above values are intended to indicate only an order of magnitude, $\bar{h}_g = 5$ Btu/hr ft^2 °F was selected. For runs 51-44 and 51-54 then, Eqs.

(4, 5, and 6) become:

Run 51-44:

$$s = 0.00895 \frac{x}{\rho_m} \tag{13}$$

$$\delta = 0.00312 \, [38.7 - x] \tag{14}$$

$$\eta = 0.6227 \tag{15}$$

Run 51-54:

$$s = 0.0120 \frac{x}{\rho_m} \tag{16}$$

$$\delta = 0.00419 \, [38.7 - x] \tag{17}$$

$$\eta = 0.6320 \tag{18}$$

In the above expressions, Θ, the time of discharge, is 88 sec for run 51-44 and 118 sec for run 51-54, and the velocity of the interface is calculated from an average discharge rate. For both runs, x = 0 is taken to be at the beginning of the cylindrical portion of the tank.

A solution of the mean cross-sectional gas-space temperature versus distance can now be obtained by a trial-and-error procedure with the addition of Eqs. (12) and (34) of Ref. 1. Eq. (12) in Ref. 1 corresponds to a step disturbance in the ambient temperature, and Eq. (34) in Ref. 1 corresponds to a linear time-dependent disturbance in the inlet temperature. The trial-and-error procedure is necessary since the mean density term, ρ_m, appears in both Eqs. (13) and (16) above. A value for ρ_m is assumed, and the gas temperature distribution is calculated and plotted. The resulting curve is integrated to obtain a value for the over-all mean temperature, from which ρ_m is calculated with use of the perfect gas law. The general procedure is outlined in detail on p. 28 of Ref. 5. The predicted mean temperatures for the conditions of run 51-54, with $T_g(\Theta_o) = 300°R$, are shown in Fig. 7, and for the conditions of run 51-54, with $T_g(\Theta_o) = 260°R$, are shown in Fig. 8. The experimental values shown are averaged values of the NASA temperature data plots of thermocouples A through F.

An evaluation of the assumptions made to obtain the solutions presented in Figs. 7 and 8 indicates that the value of $T_g(\Theta_o)$ has a significant effect on the resulting solution for the gas temperature distribution. It would be very desirable to have experimental values of temperature versus time at the location x = 0 so that fewer assumptions would be necessary in applying the theory. To show the effect of $T_g(\Theta_o)$ on the resulting gas-temperature distribution, solutions were obtained for a number of values of $T_g(\Theta_o)$ between 200°R and 400°R for the conditions of run 51-44, and are presented in Fig. 9. It can be seen that for lower values of $T_g(\Theta_o)$, the theory more closely approximates the experimental data.

Calculations for runs 95-20 and 95-23 are currently in progress. Although these two runs were obtained with the tank under conditions of sloshing, the effect of sloshing is ignored for a first approximation. It happens that for these runs the tank was only partially filled with liquid oxygen so that the thermocouple in location A is in the gas space at the beginning of discharge. Thus, the thermocouple can be considered to indicate very nearly the temperature history for the location X = 0. Solutions will be obtained and reported using this approximation.

B. Analytical Program

In previous studies,[1] dynamic response during the process of pressurized discharge of a cryogenic liquid from a container was investigated for simultaneous, multiple, time-dependent disturbances of an arbitrary form in the inlet-fluid temperature, the ambient temperature, and/or the ambient heat flux. In the formulation of the problem, the axial conduction both in the wall and pressurant could be ignored. However, when the interface-temperature difference between the pressurant and liquid increases, or when the area of this interface becomes an important fraction of the total surface wetted by the pressurant, the effect of the liquid temperature becomes equally important, and through the axial conduction, must be included in the formulation of the problem. Similarly, the interface condensation (or evaporation) may be included; this will be an important extension of the existing analytical studies.

Although as reported previously,[6] an analogical procedure has been completed which includes the effect of axial conduction, another approach—a modified integral method—is being considered as a possible method of attack for future studies.

Again, an insulated container is considered the simplest model for study in the new analysis. The transient phenomenon is introduced by the temperature difference between the pressurant and the wall.

As shown in Fig. 10a, application of the radially lumped but axially integral form of the First Law of Thermodynamics to pressurant-control volume and wall system results in (for fluid):

$$\frac{d}{d\Theta}\int_0^{V\Theta} \rho A dx c T = \rho A V c T_g - \int_0^{V\Theta} hPdx(T-t) \tag{19}$$

For wall this application results in

$$\frac{d}{d\Theta}\int_0^{V\Theta} \rho_w A_w dx c_w t = \int_0^{V\Theta} hPdx(T-t) \tag{20}$$

where A is the cross-sectional area, P the periphery, ρ the density, c the specific heat, h the heat transfer coefficient, V the velocity of pressurant, T_g the inlet temperature of the pressurant, Θ the time, x the axial distance, and subscript w the properties of the wall. The temperature of the pressurant and wall are T, t, respectively.

By introducing $b_1 = hP/\rho cA$ and $b_2 = hP/\rho_w c_w A_w$, Eqs. (19) and (20) can be rearranged in the following form:

$$\frac{d}{d\Theta}\int_0^{V\Theta} T(x,\Theta)dx = VT_g - b_1\int_0^{V\Theta} [T(x,\Theta) - t(x,\Theta)]dx \tag{21}$$

$$\frac{d}{d\Theta}\int_0^{V\Theta} t(x,\Theta)dx = b_2\int_0^{V\Theta} [T(x,\Theta) - t(x,\Theta)]dx \tag{22}$$

The rest of the problem consists of selecting suitable temperature distribution for the pressurant and wall. Here, a spatially parabolic but temporally unknown temperature profile is considered. The temperature of the pressurant is expressed in terms of the unknown interface-pressurant temperature, and the temperature of the wall is given depending on the unknown inlet-wall temperature, as shown in Fig. 10b.

Hence, the assumed profiles, with zero axial conduction on the interface, can be expressed as

$$T = T_g + (T_g - f_1)\left[\left(\frac{x}{V\Theta}\right)^2 - 2\left(\frac{x}{V\Theta}\right)\right] \tag{23}$$

$$t = f_2\left[\left(\frac{x}{V\Theta}\right) - 1\right]^2 \tag{24}$$

Substituting Eqs. (23) and (24) into Eqs. (21) and (22), and integrating Eqs. (21) and (22) with respect to x, gives

$$-\frac{2}{3}\frac{d}{d\Theta}(T_g - f_1)\Theta = b_1\left[T_g\Theta - \frac{2}{3}(T_g - f_1)\Theta + \frac{1}{3}f_2\Theta\right] \tag{25}$$

$$\frac{1}{3}\frac{d}{d\Theta}(f_2\Theta) = b_2\left[T_g\Theta - \frac{2}{3}(T_g - f_1)\Theta + \frac{1}{3}f_2\Theta\right] \tag{26}$$

By introducing the following transformation of variables

$$F_1 = (T_g - f_1)\Theta \quad , \quad F_2 = f_2\Theta \tag{27}$$

which is vitally important for a suitable solution, Eqs. (25) and (26) become

$$\frac{dF_1}{d\Theta} + b_1F_1 - \frac{1}{2}b_1F_2 = \frac{3}{2}b_1T_g\Theta \tag{28}$$

$$\frac{dF_2}{d\Theta} + b_2F_2 - 2b_2F_1 = -3b_2T_g\Theta \tag{29}$$

subject to initial conditions

$$F_1(0) = 0 \quad , \quad f_1(0) = 0 \tag{30}$$

The solution of Eqs. (28) and (29) is trivial, and can be obtained in a number of ways. Here, the following method is the most convenient. Solving, for example, Eq. (29) in terms of $F_1(\Theta)$,

$$F_2(\Theta) = b_2\int_0^{V\Theta}[2F_1(\Theta^*) - 3T_g\Theta^*]e^{-b(\Theta-\Theta^*)}d\Theta^* \tag{31}$$

is readily obtained, where Θ^* is a dummy variable. Then, substituting Eq. (31) into Eq. (28) results in an integro-differential equation in the form

$$\frac{dF_1}{d\Theta} + b_1F_1 - \frac{1}{2}b_1b_2\int_0^{V\Theta}(2F_1 - 3T_g\Theta^*)e^{-b(\Theta-\Theta^*)}d\Theta^* = \frac{3}{2}b_1T_g\Theta \tag{32}$$

The convolutive character of the integral involved in Eq. (32) suggests the use of Laplace transforms most conveniently. Hence, multiplying each term of Eq. (32) by $e^{-p\theta}d\theta$ and integrating with respect to time over the interval (o,∞) gives

$$p\bar{F}_1 + b_1\bar{F}_1 - \frac{1}{2} b_1 b_2 (2\bar{F}_1 - 3T_g \frac{1}{p^2}) \frac{1}{p+b} = \frac{3}{2} b_1 T_g \frac{1}{p^2} \tag{33}$$

where p is the Laplace transform variable. Solving $\bar{F}_1$ from Eq. (33)

$$\bar{F}_1 = \frac{3}{2} b_1 T_g \frac{1}{p^2(p+b)} \tag{34}$$

is obtained, where $b = b_1 + b_2$.

Following an identical procedure, $\bar{F}_2$ can be obtained in the following form:

$$\bar{F}_2 = \frac{3}{2} b_2 T_g \frac{1}{p^2(p+b)} \tag{35}$$

The inverse transform of Eqs. (33) and (34) is

$$\frac{F_1}{\left(\frac{3}{2}\right)b_1 T_g} = \frac{F_2}{\left(\frac{3}{2}\right)b_2 T_g} = \int_o^\theta (\theta - \theta^*) e^{-b\theta^*} d\theta^* \tag{36}$$

which gives

$$\frac{F_1}{\left(\frac{3}{2}\right)b_1 T_g} = \frac{F_2}{\left(\frac{3}{2}\right)b_2 T_g} = \frac{1}{(b_1+b_2)^2} \left[e^{-(b_1+b_2)\theta} + (b_1 + b_2)\theta - 1 \right] \tag{37}$$

Substituting Eq. (37) into Eqs. (23) and (24), the pressurant and wall temperatures are obtained in the form

$$\frac{T(x,t) - T_g}{T_g} = \left(\frac{3}{2}\right) \frac{1}{\left[1+\left(\frac{b_2}{b_1}\right)\right](b_1+b_2)\theta} \left[e^{-(b_1+b_2)\theta} + (b_1+b_2)\theta - 1 \right] \left(\frac{x}{V\theta}\right) \left[\left(\frac{x}{V\theta}\right) - 2 \right] \tag{38}$$

$$\frac{t(x,t)}{T_g} = \left(\frac{3}{2}\right) \frac{1}{\left[1+\left(\frac{b_1}{b_2}\right)\right](b_1+b_2)\theta} \left[e^{-(b_1+b_2)\theta} + (b_1+b_2)\theta - 1 \right] \left[\left(\frac{x}{V\theta}\right) - 1 \right]^2 \tag{39}$$

During the next report period, these approximate temperature profiles will be compared with the exact theory and the results of analog computations.

II. BOILING OF A CRYOGENIC FLUID UNDER REDUCED GRAVITY

A. Modifications to the Reduced-Gravity Test Facility

During the past year and a half fairly extensive data have been obtained for the boiling of liquid nitrogen from a sphere under free-fall conditions.[1,6] During operation several deficiencies in the free-fall facility became apparent, the most serious being the premature release of the test package before the test sphere had been inserted in the liquid nitrogen. On two occasions this resulted in considerable damage to the test facility.

In order to overcome this particular difficulty, to provide for more convenient calibration of the instrumentation, to provide more effectively for future modifications, and to make the system ready for operation at reduced gravity (i.e., with a counterweight), the opportunity was taken to rewire the electrical system extensively and to make the necessary mechanical revisions. These modifications are described below.

Figure 12 shows the new control panel. The upper section houses the operating switches, interlocking relays, and the various function-indicator lights for the test facility. The center section contains the thermocouple circuits, which consist of the copper knife switches and the resistors used in calibration of the records. In the lower section, housed under a hinged cover, is the 8662 potentiometer; this is used for calibration of the recorder and for direct thermocouple millivolt readings.

Figures 13-17 show the electrical control circuits and Fig. 18 presents the function of each item in the circuit. The arrangement in the control panel provides three basic modes of operation, each of which is described briefly below:

1. ONE GRAVITY TEST SUBCIRCUIT

This condition deactivates the control panel and associated interlocks, and serves primarily as an indicator during stationary or non-drop type of tests.

2. FREE-FALL TEST SUBCIRCUIT

In this mode of operation the interlocks associated with free fall and arresting of the test package are activated. Release of the test package

takes place by electrically melting the support wire. The solenoid initiating the drop is actuated by a microswitch attached to a mechanical safety hook, which is withdrawn at the desired instant of release. This redesigned safety hook, which prevents the possibility of premature release, is shown in detail in Fig. 19 and in over-all perspective in Fig. 20. The interlock circuit prevents the test package from being released by the control panel operator until:

(a) The pit cage door is closed;

(b) The buffer position is withdrawn; and

(c) The safety hook has been withdrawn at the test platform level.

3. ZERO-TO-ONE GRAVITY TEST SUBCIRCUIT

In this mode of operation the interlocks associated with the fall and arresting of both the test package and counterweight systems are activated. The test platform, counterweight, and counterweight buffer system are shown in Fig. 20. When in use, the counterweight is initially located at the lower level and connected to the test platform via a small flexible cable. Release of the test-platform counterweight system is made by a solenoid-actuated hook on the lower end of the counterweight.

The test platform is brought to a stop by the main buffer in about 3 feet of travel, whereas the counterweight is stopped by its buffer in only 8 inches. The difference in stopping distance results in cable slack and may—if the counterweight rebounds, as is possible with the air-cushioned buffer—snap the cable. To prevent rebound, four pawls are attached to the counterweight buffer to engage and hold the counterweight when contact is made with the buffer. Should the pawls not hold the counterweight and should the cable snap, a safety device is installed to prevent the counterweight from dropping to the lower level. This device consists of a rapid-action, air-cylinder-operated trap door located about a foot beneath the counterweight in its uppermost position. The trap door moves into position when the counterweight closes a microswitch upon making contact with the buffer.

The interlock circuit prevents the test-platform counterweight system from being released by the control panel operator until:

(a) The pit cage door is closed;

(b) The main buffer is withdrawn;

(c) The counterweight trap door is ready to operate;

(d) The counterweight and counterweight buffer are ready; and

(e) The safety hook has been withdrawn at the test platform level.

B. Measurement of Acceleration

In earlier presentations of experimental results,[1,6] it was stated that, based on measurements with a commercial accelerometer, the body forces on the free-fall test platform were less than 0.01g. No higher degree of precision was possible because of the limit on resolution of the instrument.

It was also pointed out that a number of correlations predict that the maximum heat flux is proportional to (a/g). For (a/g) = 0.01

$$\frac{\left(\frac{q}{A}\right)_{\max\left(\frac{a}{g}\right)=0.01}}{\left(\frac{q}{A}\right)_{\max\left(\frac{a}{g}\right)=1}} = 0.316$$

which compares to the experimental value of 0.41 reported in Ref. 1.

Proper interpretation of the experimental results requires accurate knowledge of the force field present on the falling platform. Therefore efforts are being made to measure more accurately the acceleration of the free-fall test platform.

Initially, attempts were made to obtain displacement-time data of the test package, using two accurately placed photocells and an electronic time-interval counter. The photocells were to be placed at variable vertical locations for data over the entire drop range. But computation of the platform acceleration would have required double differentiation of the displacement-time data, and errors are inherent in such a procedure.

A further difficulty was encountered: Expressing the equivalent force field present on the falling platform as a_{app}/g, it can be shown that

$$a_{app}/g = 1 - a_x/g$$

where a_x is the acceleration of the test platform. Since $a_x \approx g$ this technique involves the measurement of a small quantity from the difference of two quantities of near-equal magnitude.

To overcome these difficulties a simple accelerometer sensitive to very low values of a/g is being designed. The accelerometer consists of a small metal sphere enclosed in a housing which is attached to the test platform. By measurement of the time-displacement behavior of the sphere relative to the test platform, the force field present on the test platform can be computed directly, as indicated below. After release of the test platform the sphere is released at a specified time from the upper side of the enclosure, and the time required for it to move a small preset distance is measured. For this small distance air drag on the sphere can be neglected.

In the sketch below:

m = mass of enclosed sphere
x = position with respect to fixed coordinate system
y = position of sphere with respect to test platform

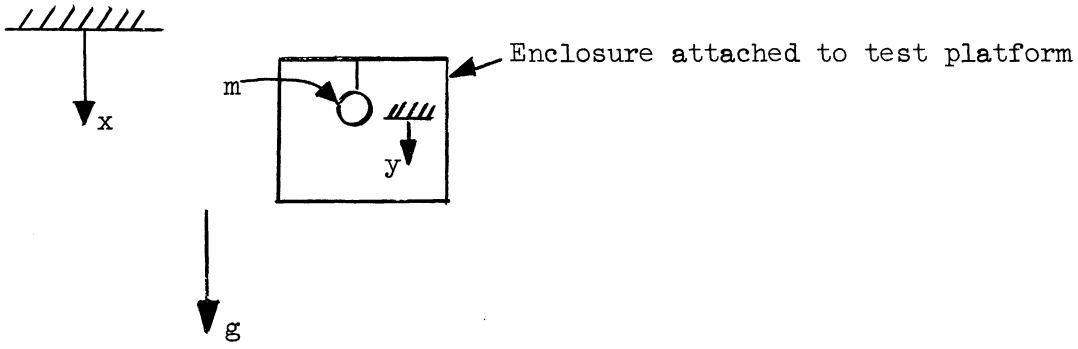

Applying Newton's Law of Motion to the sphere:

$$m\frac{g}{g_o} = \frac{m}{g_o}\frac{d^2(x+y)}{dt^2} = \frac{m}{g_o}\left(\frac{d^2x}{dt^2} + \frac{d^2y}{dt^2}\right) \tag{40}$$

If, over a short drop distance of the test platform, one considers that

$$\frac{d^2x}{dt^2} = a_x = \text{constant}$$

then

$$\frac{d^2y}{dt^2} = g - a_x \tag{41}$$

For initial conditions

$$y = 0 \quad , \quad t = 0$$

$$\frac{dy}{dt} = 0 \quad , \quad t = 0$$

integration of Eq. (41) gives

$$y = (g - a_x) \frac{t^2}{2} \tag{42}$$

or

$$a_{app}/g = \frac{2(\Delta y)}{g(\Delta t)^2} \tag{43}$$

where a_{app}/g is the dimensionless effective force field present on the falling platform and Δt is the time interval measured for the sphere to move a set distance, Δy, relative to the test platform.

The magnitude of the error introduced in assuming that a_x is constant over the drop interval Δt of the sphere will depend upon the magnitude of Δy selected. For example, if $\Delta y = 0.1$ inch and assuming that $a_{app}/g = 0.01$, then from Eq. (43) $\Delta t = 0.228$ sec. Over this time interval the test platform will move 10 inches after the moment of release, and it will move approximately 10 feet just before impact with the buffer. For the latter case the assumption of constant a_x may be erroneous. Correction can be made by using a smaller value of Δy for measurements of acceleration near termination of the test-platform motion.

The sphere is held in contact with a metallic upper plate by a 0.002-inch-diameter nichrome wire and is released by discharging a condenser through the wire. The drop interval of the sphere is measured by permitting an electrical contact between the sphere and the upper and lower plates to start and stop an electronic counter capable of time-interval measurements within 10 microseconds.

The accelerometer is currently being installed on the test platform.

C. Digital Computer Program

With the spherical test surface used for the measurement of boiling heat transfer data under conditions of free fall, a lumped system was assumed in the reduction of the data. Furthermore, it was necessary to measure the time-temperature slopes graphically.

In order to check on the validity of assuming a lumped system in the transition and nucleate boiling range and also to eliminate the necessity for graphical measurements of slopes, a numerical solution of the transient conduction process in a sphere was programmed for the IBM-709 digital computer. A finite-difference technique was used, and the experimental time-temperature measurements near the surface of the sphere served as input data. The heat flux thus determined can be compared with that obtained by the previous technique, and the computed center-surface temperature differentials compared with experimental measurements. This program greatly facilitates the reliable reduction of data and can, with minor modifications, be used for geometries other than a sphere. A brief description of the program follows.

The flow sheet showing the program logic is given in Fig. 21 and the actual program, written in the MAD (Michigan Algorithm Decoder) translator language is given in Fig. 22. The notation used is tabulated in Fig. 23.

The sphere is subdivided spatially into 10 shells of equal radial thickness, and the time interval selected is 1 millisecond. This gives an inverse Fourier modulus about twice as great as that needed to achieve stability for numerical computations with the physical system used. Computations always start with the sphere at an initial uniform temperature.

The entire set of discrete experimental time-surface temperature data (see Fig. 24) are read and stored in the computer. Since the experimental time intervals are much larger than the finite-difference time interval, intermediate values of surface temperature must be interpolated.

Five of the experimental points are taken at a time (e.g., I = 1-5 in Fig. 24) and 5 constants evaluated for Newton's interpolation polynomial. The value of C_p is calculated at the central temperature of the 5 data points (e.g., I = 3 in Fig. 24). Computation of the transient interior temperatures then proceeds from the 2nd to the 4th point; the index is then shifted 2 points, and 5 points are again used to determine a new interpolation polynomial. The procedure is continued until all the data have been processed.

When computation of the interior temperatures has proceeded to 2 steps past the central temperature of the 5 data points, the average temperature of the sphere is computed for each of 5 steps about the central temperature. A 5-constant polynomial relating average sphere temperature and time is then

determined, and the time derivative of this polynomial permits the calculation of the heat flux from the surface of the sphere.

Figure 25 is a reproduction of Fig. 50, Ref. 1, with the results of the digital computer output superimposed. This output is based on the same experimental data from which the hand computations were made. Good agreement is noted. The cost of data reduction is comparable for the two methods, but the computer greatly reduces the possibility of errors inherent in hand computations.

Heat flux and the heat transfer coefficient are plotted on linear scales in Fig. 26 to show the rapidity with which the boiling heat-transfer process passes through the transition and nucleate boiling regions. In Ref. 1 the assumption of a step change in h to 2000 Btu/hr ft^2 °F results in an analytical prediction of the maximum centerline-surface temperature difference of 2.3°F. Figure 27 shows the temperature differentials arising within the sphere for a test run in which the computer was used along with experimentally measured values. The experimental values should be compared with $t_{11} - t_2$ since the surface thermocouple was in fact located about 1/16 inches below the surface. A difference in the maximum value of 1°F is noted.

Because of the good agreement achieved by using the digital computer, it is unlikely that data reduction will be conducted by hand computations in the future.

D. Future Work

Should the measurements of acceleration indicate that the effect of air drag on the free-fall test package is appreciable, it may be desirable to replace the present test package with a more streamlined one. (A more streamlined package is currently available.) In case of replacement, several test runs with the sphere under free-fall conditions will be repeated to observe if changes in the basic data occur. It is possible that some of the scatter in the free-fall film boiling data is a direct consequence of the variable air drag on the test package.

Data will also be obtained with the sphere under frictional gravity, making use of the counterweight system.

A flat plate disc heating surface, currently available, will then be used to study the influence of surface orientation under fractional gravity conditions.

III. HEAT TRANSFER TO A CRYOGENIC FLUID IN AN ACCELERATING SYSTEM

The skirt-guard heater in the test vessel has been repaired and steps taken to minimize the possibility of further burnout.

The test vessel was installed in the centrifuge to obtain boiling heat-transfer data with system acceleration. Difficulties were encountered in obtaining temperature measurements. It was found that portions of the rotating iron wires inserted in the mercury commutator rings had become coated with some type of deposit which served to partially insulate the wires. After 3 years of operating the centrifuge, the deposit is probably an accumulation of surface scum on the mercury. Because the electrical insulation on the wires connecting the mercury slip rings to the test vessel appeared in questionable condition, the wires were replaced.

Opportunity was also taken to recalibrate the thermocouples by vapor-pressure measurement in a pure nitrogen liquid-vapor equilibrium vessel. A slight deviation from the previous calibration was observed.

Several tests were conducted under acceleration with liquid nitrogen in the test vessel but with no power input to the heaters in order to become familiar with operational procedures.

A. Test Procedures

Since the present centrifuge has no facilities for transferring liquid nitrogen to the test vessel while under rotation, the test vessel must be filled just prior to rotation and measurements taken while the liquid level remains high enough for safe operation. Thus the mass of the rotating test vessel will change with time. A counterweight filled with water was designed in such a manner that by a programmed discharge of the water, dynamic balance could be maintained at all times. However, it became apparent that it would be difficult to synchronize the rate of discharge of water with the boiloff rate of liquid nitrogen. The counterweight is now adjusted so that dynamic balance is achieved with the test vessel half filled with liquid. The unbalance occurring when the test vessel is full or near empty has caused no difficulty in operation.

A styrofoam float with a scale indicator is installed in the test vessel for liquid-level measurements. Since this reading can be made only under

non-rotating conditions, a single heated carbon resistor is used in conjunction with a milliammeter to indicate, under rotation, when the depth of the liquid reaches approximately 1 1/2 inches.

The center-heater temperature is measured with respect to an ice point by a thermocouple located 1/16 inches below the surface, and the surface temperature obtained by extrapolation from this reading. A second thermocouple in the heater surface serves to check temperature uniformity. Liquid temperatures are measured at 1/4 inches and 1 5/16 inches from the heater surface. A differential thermocouple is installed between the underside of the heater and the lower guard heater. This has always indicated differences of less than 2°F with no power on the guard heater. Another differential thermocouple is installed between the heater surface and the skirt guard heater. The differential is maintained at less than 1°F by adjustment of the power input to the skirt-guard heater, and reduces heat loss by conduction from the skirt estimated to be less than 3% of the total main-heater power input. The locations of the differential thermocouples and guard heaters are shown in Fig. 76 of Ref. 1.

A vent tube was added to the test vessel to carry the boiloff vapor to a point near the center of rotation in order to avoid a pressure change within the vessel during rotation.

Liquid nitrogen purity was measured at least once during each test, with the impurity assumed to be oxygen.

In each of the test runs the heat flux was held constant while the acceleration was varied. In order to establish the effect of acceleration more accurately, particularly when boiling characteristics change with time, a set of readings has been taken at $a/g = 1$ before and after each change of acceleration.

B. Test Results

Tests had been conducted at 3 values of heat flux with accelerations up to $a/g = 18.3$, when a short circuit developed in the main heater. Upon disassembly it was found that the screws connecting the heater assembly to the inner vessel sidewalk had become loose, with the possibility that a leakage of liquid nitrogen from the inner test vessel could have occurred. How this may have affected the results is uncertain, since the leakage path is outside the lower heater container. However the results presented below should be considered tentative until additional data are available.

Since liquid level could be measured at only one point while under rotation, the levels shown are derived from the one measurement in conjunction

with float level readings taken immediately preceding and following rotation, and are the best estimates possible.

RUN NO. 21. $q/A = 10{,}150$ Btu/hr-ft^2

Figure 28 shows the temperature data taken as a function of elapsed time. The decrease in the heater surface and fluid temperatures with decrease in depth is noted, indicating the influence of a decrease in hydrostatic head. However, the values of $(T_{surface} - T_{sat})$ remain almost constant.

To indicate more clearly the influence of varying liquid depth, the temperatures and local saturation temperature differences are plotted in Figs. 29-32 for each acceleration. At the left of the figures the heater surface and fluid temperatures are plotted along with computed local saturation temperatures. At the right of the figures the differences between the measured temperatures and local saturation temperatures are indicated. Note that $(T_{surf} - T_{sat\ (local)})$ is not influenced by small changes in pressure.

Figure 33 is a composite plot of local saturation temperature differences as a function of acceleration for a particular depth of liquid. With reference to the upper curves, $T_{surf} - T_{sat}$ increases with an increase in acceleration, whereas the superheat of the liquid decreases. It is also noted that with time, a small shift in the data occurs at $a/g = 1$. This shift is eliminated in the lower curves by plotting only changes between the values at $a/g = 1$ and higher accelerations.

RUN NO. 22. $q/A = 20{,}100$ Btu/hr-ft^2

The data for a higher heat flux in Figs. 34-39 are presented in the same manner as the comparable data for run no. 21. In Fig. 34 the heater surface temperature undergoes a period of instability after the initial acceleration. A similar phenomenon has been noted in other test runs, but as yet no explanation can be given.

As with run no. 21, Fig. 40 shows that $(T_{surf} - T_{sat\ (local)})$ increases with an increase in acceleration.

RUN NO. 23. $q/A = 5{,}020$ Btu/hr-ft^2

Figure 41 is the time-temperature data at a low level of heat flux. An instability after the first rotation is again noted. In accounting for the rather severe shift in temperatures after rotation at $a/g = 18.3$, it was found that the nitrogen vapor efflux had been accidently directed at the mercury channels, with non-uniform temperatures probably inducing extraneous EMF's.

Figure 42 is a composite plot of the saturation temperature differences as a function of acceleration. $T_{surf} - T_{sat}$ experiences a slight rise and then a decrease with increasing acceleration. A similar phenomenon observed with water (Ref. 7) at low values of heat flux was attributed to the increasing contribution of non-boiling convective heat transfer.

In each of the test runs above, the liquid is superheated somewhat at $a/g = 1$ and the superheat decreases with increasing acceleration. Also, for example in Fig. 41, at accelerations above about $a/g = 6$ the liquid attains a uniformity in temperature. At the highest acceleration of $a/g = 18.3$ the thermocouples indicate that the liquid nitrogen is saturated near the heating surface and superheated at a distance away from the heating surface. The bulk-liquid temperature thus tends to be near the saturation temperature at the heating surface. With water (Ref. 7) it was found that the bulk-liquid temperature tended to be closer to the saturation temperature corresponding to the liquid-vapor interface, and somewhat subcooled at the heater surface. The difference in behavior is thought to be caused by the difference in experimental techniques. With water, the vapor generated is condensed and returned saturated to the bulk liquid. The reflux assists in maintaining the bulk liquid at the saturation temperature of the liquid-vapor interface. With liquid nitrogen, the vapor generated is removed from the system completely; and since intense convection is present due to acceleration, heating the bulk liquid from below would tend to keep the bulk-liquid temperature near that of the liquid at the heating surface (i.e., near saturation).

C. Future Work

After the main heater has been repaired, additional data will be obtained at various accelerations and values of heat flux up to approximately $q/A = 30{,}000$ Btu/hr-ft^2 in the same manner as that presented here. A number of tests will also be conducted at $a/g = 1$ but with various values of heat flux to serve as a base for comparison with data of the system under acceleration.

It is planned that an auxiliary heater will be designed for installation in the present test vessel to study the effect of acceleration for the case where the acceleration vector is parallel to the heating surface. A preliminary sketch of the proposed heater was given in Ref. 5.

IV. INJECTION COOLING

A. Lumped System

1. INTRODUCTION

In a previous study[6] the lumped-system analysis of the injection cooling process was developed to a generally satisfactory form. A summary is given here for the complete system transient in response to the injection of a highly soluble gas, and the previous analysis is extended to include variable gas enthalpy flux.

2. SUMMARY OF THE SYSTEM TRANSIENT

For a full understanding of the system-transient behavior in response to ambient heating and a period of gas injection, a summary is given for the general case of the injection of a highly soluble gas. The quantitative description is based on the analysis and nomenclature presented in Ref. 6, and the form is such that account can be made for a variable gas enthalpy flux and arbitrary equilibrium approximation. Figure 43 shows a schematic of the six characteristic stages of the thermal lumped-system transient.

a. Ambient Heating

Assuming the system initially contains subcooled pure liquid of component A, the ambient heating causes a linear system temperature rise according to

$$\dot{\Theta} = B \tag{44}$$

If the saturation state is reached, boiling occurs along the walls of the column, and $\dot{\Theta} = 0$.

b. Liquid Displacement Transient

As discussed in Ref. 6, p. 18, a nearly constant gas hold-up volume is established in the system after gas injection is initiated. There is experimental evidence[8] that the duration of this liquid displacement transient is short compared with the period of gas injection. Figure 44 shows the differential pressure measurement over a fixed length of an experimental column[8]

during gas injection. Although it has not been substantiated that the upper pressure sensor was at all times covered by liquid-gas mixture, the data are indicative for at least the initial transient. This stage of the gas injection is considered to have no effect on the system temperature.

c. Gas Injection with Only Liquid Phase Present

If the saturation temperature is not reached when gas injection is initiated, all the injected gas of component B is absorbed in the liquid until the liquid composition has reached that of equilibrium corresponding to the prevailing system temperature. This process is associated with system heating rather than cooling, according to Eq.(45) [cf. Ref. 6, Eq. (11)]

$$\dot{\Theta} = A \frac{1 + LZ}{1 + KZ} (F + C) + B \tag{45}$$

d. Gas Injection with Two-Phase Equilibrium (Evaporative Cooling)

This phase of the injection process has been the main object for the previous investigation since it provides the desired cooling. The transient is approximately described by Eq. (39) of Ref. 6:

$$\left\{1 + \frac{E[\frac{1}{X} + F]}{1 + KZ} \left[-\left(\frac{\partial Z}{\partial \Theta}\right)_p\right]\right\} \dot{\Theta} = A \cdot \frac{1 + LZ}{1 + KZ} \cdot \frac{[-\frac{1}{X} + C]}{[1 - G(1 + \frac{1}{X_\infty})]} + B \tag{46}$$

e. Back-Flow and Mixing

When gas injection is terminated, liquid (comprised essentially of pure component A) flows back from the reservoir and fills the column, undergoing some mixing with the liquid remaining in the column. If the liquid in the reservoir is colder than that in the system, some cooling is produced in the upper portion of the system. However, within the frame of the lumped-system analysis, full mixing is assumed such that the back-flow—being of short duration—results in a sudden temperature drop, as illustrated in Fig. 43. If the reservoir temperature is Θ_r and gas injection is terminated when the system is at temperature Θ_2, the resulting temperature Θ_3, following adiabatic mixing, is determined from

$$\frac{\Theta_2 - \Theta_3}{\Theta_3 - \Theta_r} = \frac{G}{1 - G - \Theta_2} \cdot \frac{1 + LZ}{1 + KZ} \tag{47}$$

In Eq. (47) the gas hold-up volume has been based on state 2 (Fig. 43) rather than on the asymptotic state; hence $V_G/V_L = G(1 + 1/X_2)/[1 - G(1 + 1/X_2)]$, or with the linear approximation for the dew-curve, $\Theta = x$, $V_G/V_L = G/(1 - G - \Theta_2)$.

It should be noted that Eq. (47) is not necessarily valid if $\Theta_r > \Theta_2$, since the resulting temperature Θ_3 in this case might exceed the boiling temperature of the mixture.

f. Ambient Heating of Subcooled Two-Component Mixture

Following the mixing, the lumped-system temperature rises linearly according to $\dot{\Theta} = B$, until the saturation temperature Θ_4 is reached, corresponding to the liquid composition

$$Z_4 = \frac{1 - Z_4}{Z_4} = \frac{Z_2}{1 + G(1 + LZ_2)/(1 - G - \Theta_2)} \tag{48}$$

g. Ambient Heating of Saturated Two-Component Mixture (Fractional Distillation)

Subsequently the rate of temperature rise owing to ambient heating will be reduced, since the more volatile component B distills off the mixture. During this process the liquid composition is assumed to be that of phase-equilibrium corresponding to system temperature. Since the volume of vapor formed is small, the lumped-system temperature can be described by Eq. (46) for $A = 0$:

$$\left\{1 + \frac{E\left(\frac{1}{X} + F\right)}{1 + KZ}\left[-\left(\frac{\partial Z}{\partial \Theta}\right)_p\right]\right\}\dot{\Theta} = B \tag{49}$$

Eq. (49) indicates that the rate of temperature rise may be reduced by an order of magnitude.

The injection of gaseous nitrogen into liquid oxygen is an example of injection cooling for which a non-condensing gas of high solubility is used. The average (lumped) system temperature for Experiment No. 93-29 reported in Ref. 9 is plotted in Fig. 45. The experimental data indicate the occurrence of most of the stages discussed above, though the back-flow and subsequent ambient heating are not fully substantiated. Lack of detailed information on reservoir conditions have prevented quantitative comparison with theory. However, stages C and D of the injection transient have been compared with theory, using the integrated forms of Eqs. (45) and (46) respectively and employing linear equilibrium approximations [cf. Eqs. (31) and (32) in Ref. 6]. The observation that the experimental cooling rate exceeds the predicted rate seems to indicate that the gas-to-liquid mass transfer rates are insufficient to establish equilibrium compositions in the liquid phase. Liquid-to-gas mass transfer, however, occurs at a rate sufficient to create a net cooling effect.

While the axial temperature distribution in the liquid oxygen in the column shows a temperature drop of about 1°F from bottom to top for the case

of helium injection, the difference is nearly 3°F for Experiment No. 93-29 (Ref. 9) for nitrogen injection. Hence a significant axial concentration distribution can be expected to exist in this case. The shortcomings of the lumped analysis can be circumvented by predicting an effectively attainable average liquid composition, formally given by a non-equilibrium value of ϵ. Governing factors would be injection pattern, gas flow rate, and system geometry. An empirical correlation may be possible when sufficient experimental data have been reduced. However, bubble dynamic studies are expected to permit theoretical correlation either by extending the lumped-system model or by considering an axially-distributed system. For Experiment No. 93-29, Fig. 45, a value of $\epsilon = 0.17$ gives good correlation compared with the equilibrium value of 0.333.

In view of the particular application of the injection cooling process it should be noted that the use of a highly soluble gas is undesirable for the following reasons:

(1) Only low subcooling can be attained.

(2) Subsequent to gas injection and liquid back-flow, a saturated two-component mixture is soon established (stage g), and this facilitates flashing when the pump suction head is imposed on the system.

(3) The two-component mixture formed in the system may have undesirable properties.

The use of a soluble gas seems applicable only if advantage is taken of the liquid exchange with the reservoir. Hence, if gas injections of very short duration are performed—which prevent considerable contamination of the liquid but are sufficient to displace a reasonable fraction of the liquid out of the column—a satisfactory subcooling can be obtained, provided no structural damage results from liquid hammer effects.

3. VARIABLE GAS ENTHALPY FLUX

In the previous analysis[6] the gas enthalpy flux appearing in the property group $C = \Delta h_B/h_{fgA} = c''_B(T_{Bi}-T)/h_{fgA}$ was assumed constant. This assumption is nearly correct for small temperature changes in cryogenic systems if the initial gas temperature, T_{Bi}, is that of the ambient. However, when the injected gas is precooled nearly to system temperature and its heat capacity is not negligible, C must be considered a variable. Assuming the molal specific heat, c''_B, of the gas to be constant, C can be written in terms of the constant C' defined by

$$C = \frac{\Delta h_B}{h_{fgA}} = \frac{c''_B(T_A - T_B)}{h_{fgA}}(\Theta_B - \Theta) = C'(\Theta_B - \Theta) \qquad (50)$$

where $\Theta_B = (T_{Bi} - T_B)/(T_A - T_B)$.

Hence, for the asymptotic temperature for low solubility of the injected gas, Eq. (35) of Ref. 6 is replaced by

$$x_\infty = \frac{(1 - G)\, B/A + C'(\Theta_B - \Theta)}{1 + B/A + C'(\Theta_B - \Theta)} \tag{51}$$

If the linear equilibrium approximation, $x = \Theta$, is retained, Θ_∞ is determined from

$$\Theta_\infty^2 - \frac{1 + B/A + C'(1 + \Theta_B)}{C'}\,\Theta_\infty + \frac{(1 - G)B/A + C'\Theta_B}{C'} = 0 \tag{52}$$

Under the assumption of linear equilibrium approximations and dilute solutions the approximate transient solution, Eq. (41) of Ref. 6, is replaced by

$$\frac{M - \Theta_I}{\Theta_I - \Theta_{II}}\,\ell n\,\frac{\Theta - \Theta_I}{\Theta_o - \Theta_I} - \frac{M - \Theta_{II}}{\Theta_I - \Theta_{II}}\,\ell n\,\frac{\Theta - \Theta_{II}}{\Theta_o - \Theta_{II}} = \frac{A_1 C'}{1 - \epsilon E(1 - F)}\,t \tag{53}$$

where Θ_I and Θ_{II} are the roots in Eq. (52) and the property group $M = [1 + \epsilon EF]/[1 - \epsilon E(1 - F)]$.

The cooling of liquid hydrogen by the injection of gaseous helium precooled to liquid hydrogen temperatures is an example where variable gas enthalpy flux may be considered. Based on tentative phase-equilibrium data, however, a correlation of experimental results from the recent measurements by Schmidt[10] indicates that consideration of the enthalpy flux variable causes a change of only a few percent in the asymptotic temperature.

In general it has not yet been possible to obtain satisfactory correlation between the lumped-system analysis and the available experimental data for the hydrogen-helium system, except for the case of low subcoolings. The tentative phase-equilibrium data, obtained from vapor-pressure data for the pure substances, is believed to be inaccurate in the region of high relative subcooling. For future work, reliable measured equilibrium data seem to be required, especially near the region of solid-hydrogen temperatures.

B. Bubble Dynamics

1. INTRODUCTION

An outline of the studies anticipated in connection with the injection cooling process is given in Ref. 1, p. 40. A study of the discrete processes of mass and heat transfer to the rising bubbles of the injected gas is necessary for the development of an analysis of the axially distributed system. By this extension of the lumped analysis, the assumption of an equilibrium process is shifted from the macroscopic level to the microscopic level, viz., from instantaneous equilibrium throughout the system at all times to thermodynamic phase-equilibrium at all times at the bubble interface.

First the dynamics of a single bubble and then ensembles of bubbles will be studied. As the limiting case for very high transfer rates, the motion of the bubble with associated nonradial fluid flow can be ignored, and the bubble dynamics can be approximated by that of a stationary bubble. When transfer rates are small, however, the translatory motion of the bubble needs to be considered.

Analytical and experimental studies are currently in progress for the dynamics of a single bubble, initially containing a nonsoluble gas and having no translatory motion in the surrounding volatile liquid.

2. ANALYSIS

The first stage of bubble dynamic study is stated as follows in Ref. 1, p. 51: "The dynamics of a single spherical bubble having no translatory motion and containing a nonsoluble, noncondensable and chemically nonreactant gas and the vapor of a volatile liquid of infinite extent which surrounds the bubble." The physical model discussed in Ref. 1, p. 51 ff. and in Ref. 6, p. 33 ff. will be extended to include the assumption that the composition of the gas phase is uniform at all times. This is a reasonable assumption if the rate of mass diffusion in the gas phase is high compared with the rate of heat diffusion in the surrounding liquid. The uniform gas composition in conjunction with phase-equilibrium requirements at the bubble interface relates the bubble size directly to the interface temperature. The problem is thus reduced to that of spherical bubble growth, governed by heat conduction and convection in the surrounding liquid, and having a prescribed initial size and varying interface temperature.

The heat diffusion problem is solved with the aid of source theory, as outlined in Ref. 6, p. 28 ff. The following general approximate solution is obtained, relating the differential change of the interface temperature, dT_s,

and the corresponding differential change in bubble size, dR, [Ref. 6, Eq. (51)]

$$d(T_b - T_s) = \frac{\delta}{\sqrt{\pi\,\alpha}} \frac{R(y)\,\dot{R}(y)\,dy}{R(t)\sqrt{t - y}} \tag{54}$$

where the property group $\delta = (h_{fg}v')/(c'v'')$, y is a time between t = 0 and t = t, α is the thermal diffusivity, T_b is the bulk temperature of the liquid far from the bubble, and a dot ($\dot{}$) signifies differentiation with respect to time. Any variation of T_s is retained in the subsequent integration from t = 0 and R = R_o to t = t and R = R. Introducing the nondimensional quantities

$$\tau = \alpha t/R_o^2$$

$$P = R/R_o$$

$$\Theta = (T - T_B)/(T_A - T_B)$$

$$\lambda_o = (T_A - T_B)/\delta$$

where $T_A - T_B = (\partial T/\partial x)_p$ is the slope of the linear approximation to the dew curve, integration of Eq. (54) gives

$$\sqrt{\pi}\,\lambda_o(\Theta_b - \Theta_s)\,P(\tau) = \int_0^\tau \frac{P(y)\,\dot{P}(y)}{\sqrt{\tau - y}}\,dy \tag{55}$$

Noting that the integral is a convolution, Eq. (55) may be written,

$$2\sqrt{\pi}\,\lambda_o(\Theta_b - \Theta_s)\,P = (\dot{P}^2) * \frac{1}{\sqrt{\tau}} \tag{56}$$

For constant interface temperature and initial zero bubble size, Eq. (56) describes the approximate bubble growth in a boiling, one-component liquid. The solution $P = 2\lambda\sqrt{\tau}$, where $\lambda = (\sqrt{\pi}/2)(\Theta_b - \Theta_s)\lambda_o$, is easily verified by substitution and Laplace operation on Eq. (56). When the interface temperature is an arbitrary function of bubble size, numerical integration is necessary. By introducing an additional approximation, however, Eq. (56) can be linearized and closed-form solutions obtained. Considering the gas phase an ideal mixture and assuming a linear phase-equilibrium approximation for the dew curve, x = Θ, continuity considerations give:

$$P^3 = \frac{1}{1 - x_s} = \frac{1}{1 - \Theta_s} \tag{57}$$

Substituting Eq. (57) into Eq. (56) gives

$$2\sqrt{\pi}\,\lambda_o[1/P^3 - (1 - \Theta_b)]P = (\dot{P}^2) * \frac{1}{\sqrt{\tau}} \tag{58}$$

Eq. (58) is linearized by the approximation

$$2\,\lambda_o(\Theta_b - \Theta_s) = 2\,\lambda_o[1/p^3 - (1 - \Theta_b)] \cong a/P - bP \tag{59}$$

where a and b are constants. Thereby Eq. (58) can be operated on by Laplace transformation, resulting in the closed form solution

$$P(\tau) = \sqrt{\frac{a}{b} - \left(\frac{a}{b} - 1\right) \cdot \exp b^2\tau \cdot \operatorname{erfc} b\sqrt{\tau}} \tag{60}$$

Figure 46 shows the interface temperature versus bubble size as given by Eq. (57) for different values of the initial bulk liquid subcooling, $\Delta\Theta_{sub} = 1 - \Theta_b \cdot (\Theta_b - \Theta_s)$ being the potential for bubble growth, this ceases when $\Theta_s = \Theta_b$, giving the asymptotic bubble size as

$$P_\infty = \frac{1}{\sqrt[3]{1 - \Theta_b}} \tag{61}$$

Hence, a nonsoluble gas bubble would grow continually if injected into a saturated liquid ($\Theta_b = 1$) extending to infinity. As the subcooling is increased the asymptotic size rapidly decreases towards unity, the initial size.

The approximation given by Eq. (59) is shown by the dotted lines in Fig. 46. For the cases of the nondimensional subcooling $\Delta\Theta_{sub}$ being different from zero, the constants a and b are fitted to satisfy the conditions

$$P = 1 : \quad \Theta_s = 0$$

$$P = P_\infty : \quad \Theta_s = \Theta_b$$

This gives

$$a = \frac{2\lambda_o\Theta_b}{1 - (1 - \Theta_b)^{2/3}} \tag{62}$$

$$b = \frac{2\lambda_o\Theta_b(1 - \Theta_b)^{2/3}}{1 - (1 - \Theta_b)^{2/3}} \tag{63}$$

As seen from Fig. 46 the approximation becomes less and less satisfactory as the subcooling decreases. For the case of a saturated bulk liquid, $\Delta\Theta_{sub} = 0$, only the initial bubble growth can be approximated by a single set of constants a and b, for example, satisfying the two initial conditions

$$P = 1: \quad \Theta_s = 0$$

$$P = 1: \quad \frac{\partial}{\partial P}\{2\lambda_o[1/P^3 - (1 - \Theta_b)]\} = \frac{\partial}{\partial P}\{a/P - bP\}$$

This gives

$$a = \lambda_o(3 + \Theta_b) = 4\lambda_o \tag{64}$$

$$b = \lambda_o(3 - \Theta_b) = 2\lambda_o \tag{65}$$

Relative nondimensional bubble growth, $Q = (P - P_o)/(P_\infty - P_o)$, where $P_o = 1$ and P and P_∞ are given by Eqs. (60) and (61), is shown in Fig. 47. The relative bulk subcooling $\Delta\Theta_{sub} = 1 - \Theta_b$ is a parameter and an arbitrary value of $\lambda_o = 12.6$ has been chosen which corresponds to liquid oxygen at 184°R and 1.3 atm. As the subcooling increases a certain fractional growth is attained in successively shorter nondimensional times. The absolute time-constant for the discrete process of bubble growth is thus seen to decrease with increasing subcooling and decreasing initial bubble size. At the same time the absolute bubble growth also decreases [cf. Eq. (61)]. However, the integrated heat transfer per unit gas volume injected initially decreases with increasing initial subcooling and increasing initial bubble size, as seen from the expression for a single bubble of initial volume V_B:

$$\frac{Q}{V_B} = \frac{(4/3) \cdot \pi \cdot (R^3 - R_o^3) \cdot (h_{fg}/v'')}{(4/3) \cdot \pi \cdot R_o^3}$$

or

$$\frac{Qv''}{h_{fg}V_B} = P^3 - 1 \tag{66}$$

For the case of finite subcooling, where the approximation in Eq. (59) holds, the variable bubble Nusselt number $Nu_b = hR_o/k$ becomes

$$Nu(\tau) = \frac{1}{b}\frac{\partial}{\partial\tau}\left\{\ell n\left[\left(\frac{a}{b} - 1\right) \cdot \exp b^2\tau \cdot \operatorname{erfc} b\sqrt{\tau}\right]\right\} \qquad (67)$$

where the coefficient of heat transfer, h, is arbitrarily defined by

$$q = h \cdot (4\pi R^2) \cdot (T_b - T_s) \qquad (68)$$

Figure 47 indicates the slow relative growth for small subcooling and reasonable (1/16 inches to 1/4 inches diameter) initial bubble size. Since for liquid oxygen $\alpha = 0.00073$ cm^2/sec, $\tau = 0.0073$ corresponds, for example, to t = 1 sec and R_o = 1/8 inches. The relative growth also expresses to what degree the equilibrium composition and size is reached at any time.

Despite the many assumptions made in the present analysis, the order of magnitude and trend of the results are considered representative for the growth rates of stationary, inert gas bubbles in a volatile liquid. In view of the satisfactory results obtained from the lumped analysis, which assumes instantaneous equilibrium, it may be concluded that the translatory motion of the bubbles with associated nonradial convective flow in the liquid plays a significant role in the transfer of mass and heat.

3. EXPERIMENTAL PROGRAM

Construction of apparatus is in progress for the experimental study of the dynamics of a single bubble having no translatory motion. Figure 48 shows the apparatus. A view tank 1 x 1 1/2 feet, constructed from stainless steel channels and having Pyrex glass sides, holds the volatile liquid, which is heated by a 1-kw immersion heater. The bubble injector and a 1/8-inch copper tubing coil gas preheater are mounted on the tank lid, which can be sealed to the tank top to permit operation at pressures slightly different from atmospheric pressure. This arrangement also permits a controlled atmosphere to be maintained over the liquid.

The bubble injector is shown in detail in Fig. 49. A 6-V, DC, 24-oz solenoid L with adjustable core stop K for the plunger M, is mounted on the top plug E in the cylindrical 1 3/4 inch O.D. brass casing H. The solenoid plunger M is connected to the valve P, which is seated near the tip of the nozzle R by means of the spring S. Gas from the preheater coil is supplied at the fitting T to the inside of the casing, which is sealed at all joints with O-rings and which can be vented to the atmosphere through a 1/4-inch tubing soldered to the top plug.

Through an adjustable electric switching circuit the solenoid is energized for a short period of time, during which a gas bubble is formed at the nozzle tip. Adjustment of valve stroke, energizing of time and voltage,

spring tension, and gas pressure permit the desired initial bubble size to be attained. By pickup of the induced voltage drop over the solenoid coil, the plunger motion can be monitored by a high-speed recording instrument, giving information on the bubble injection time. Two nozzles with matching valves are being made which have nozzle diameters of 1.5 mm and 3.0 mm respectively. The bubble growth subsequent to injection will be recorded by high-speed moving pictures. The case of a nonsoluble gas will be studied first, using nitrogen injected into nitrogen-saturated distilled water at various subcoolings at near atmospheric pressures.

The bubble injector is nearly completed and materials for the view tank are arriving.

REFERENCES

1. Clark, J. A., H. Merte, Jr., V. S. Arpaci, et al., Pressurization of Liquid Oxygen Containers, Univ. of Mich. ORA Report 04268-2-P, Ann Arbor, Nov., 1961.

2. McAdams, W. H., Heat Transmission, 3rd Edition, McGraw-Hill, New York, 1954.

3. Kreith, F., Principles of Heat Transfer, Int. Textbook Co.

4. Van Grundy, D. A. and J. R. Uglum, "Heat Transfer to an Uninsulated Surface at 20°K," Advances in Cryogenic Engineering, 7, K. D. Timmerhaus, Editor, Plenum Press, 1962.

5. Clark, J. A., H. Merte, Jr., V. S. Arpaci, et al., Pressurization of Liquid Oxygen Containers, Univ. of Mich. ORA Report 03583-3-F, Ann Arbor, March, 1961.

6. Clark, J. A., H. Merte, Jr., V. S. Arpaci, et al., Pressurization of Liquid Oxygen Containers, Univ. of Mich. ORA Report 04268-3-P, Ann Arbor, March, 1962.

7. Merte, H., and J. A. Clark, "Pool Boiling in an Accelerating System," Trans. ASME, J. Heat Transfer, 83, 3, pp. 233-242, 1961.

8. "Cryogenic Subcooling by Helium Injection," George C. Marshall Space Flight Center, Memorandum M-S&M-PE No. 327, Oct. 24, 1961.

9. W. J. Halbrooks, "Tests of Cryogenic Cooling by Gaseous Injection," MSFC Internal Note M-Test No. 13-61, August 10, 1961.

10. Schmidt, A.F., "Experimental Investigation of Liquid Hydrogen Cooled by Helium Gas Injection," NBS Cryogenic Engineerying Laboratory, Boulder. (Paper J-4, 1962 Cryogenic Engineering Conference).

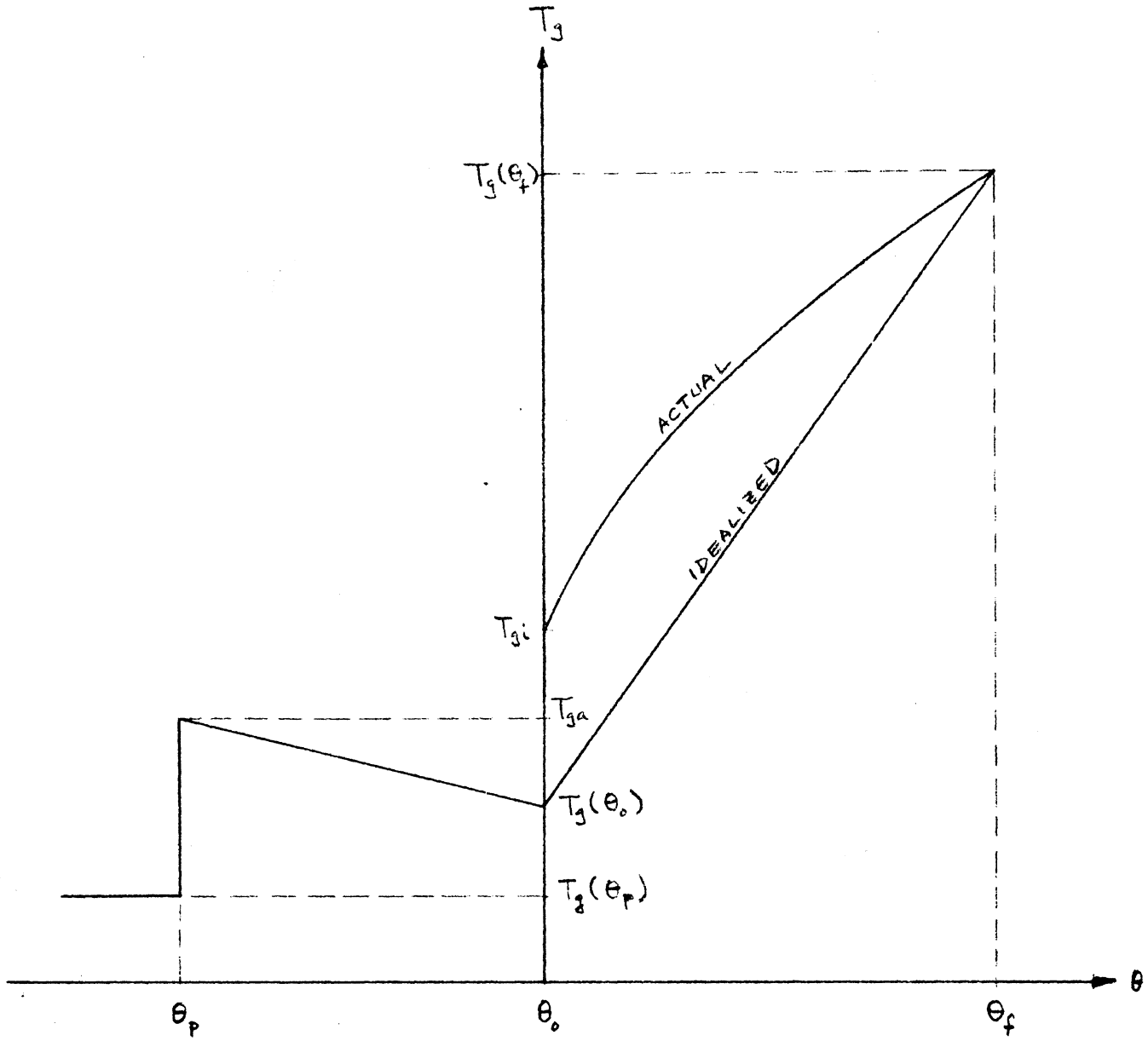

FIG. 4. IDEALIZED TIME-INLET GAS TEMPERATURE CURVE

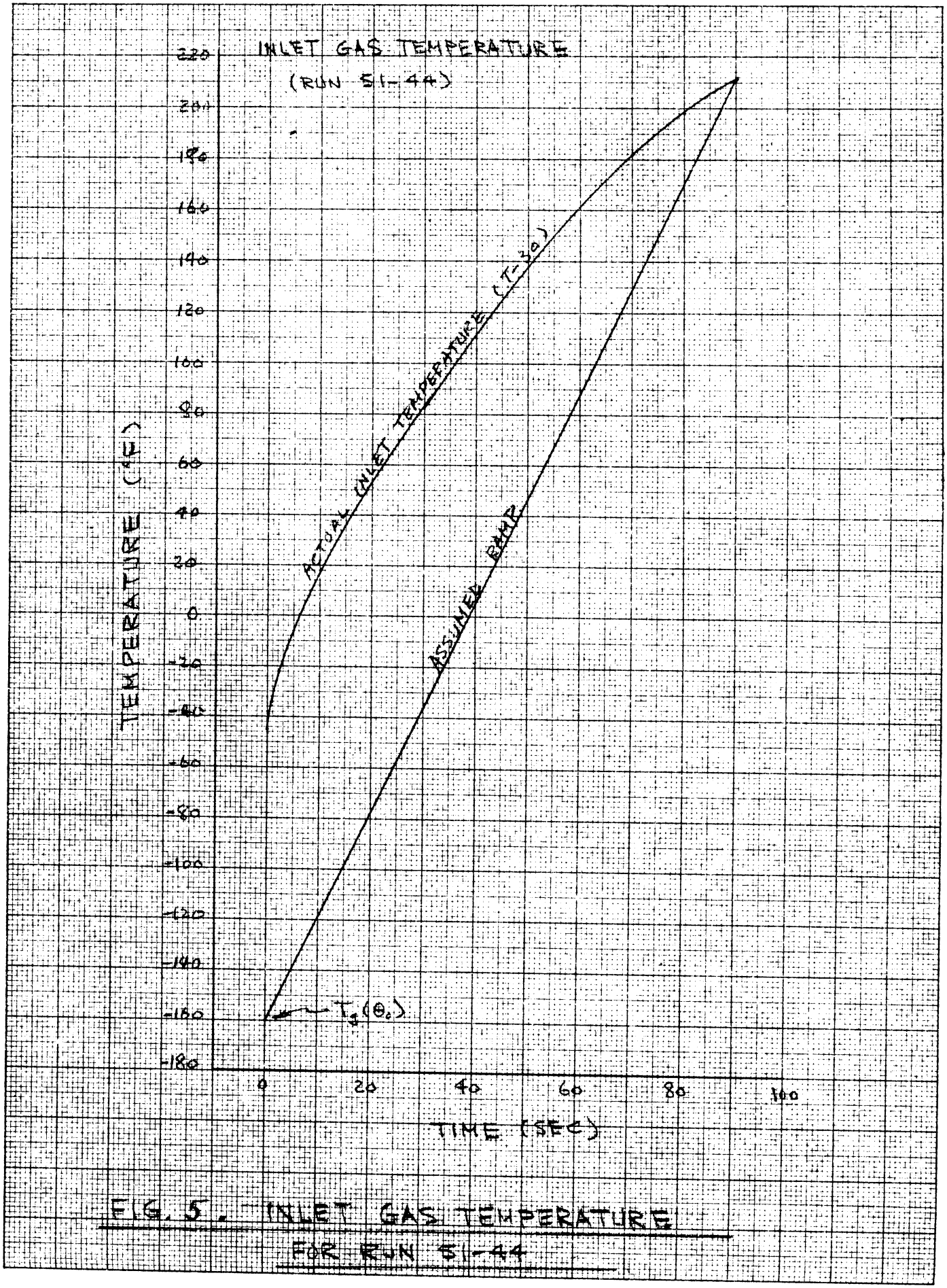

FIG. 5. INLET GAS TEMPERATURE FOR RUN 51-44

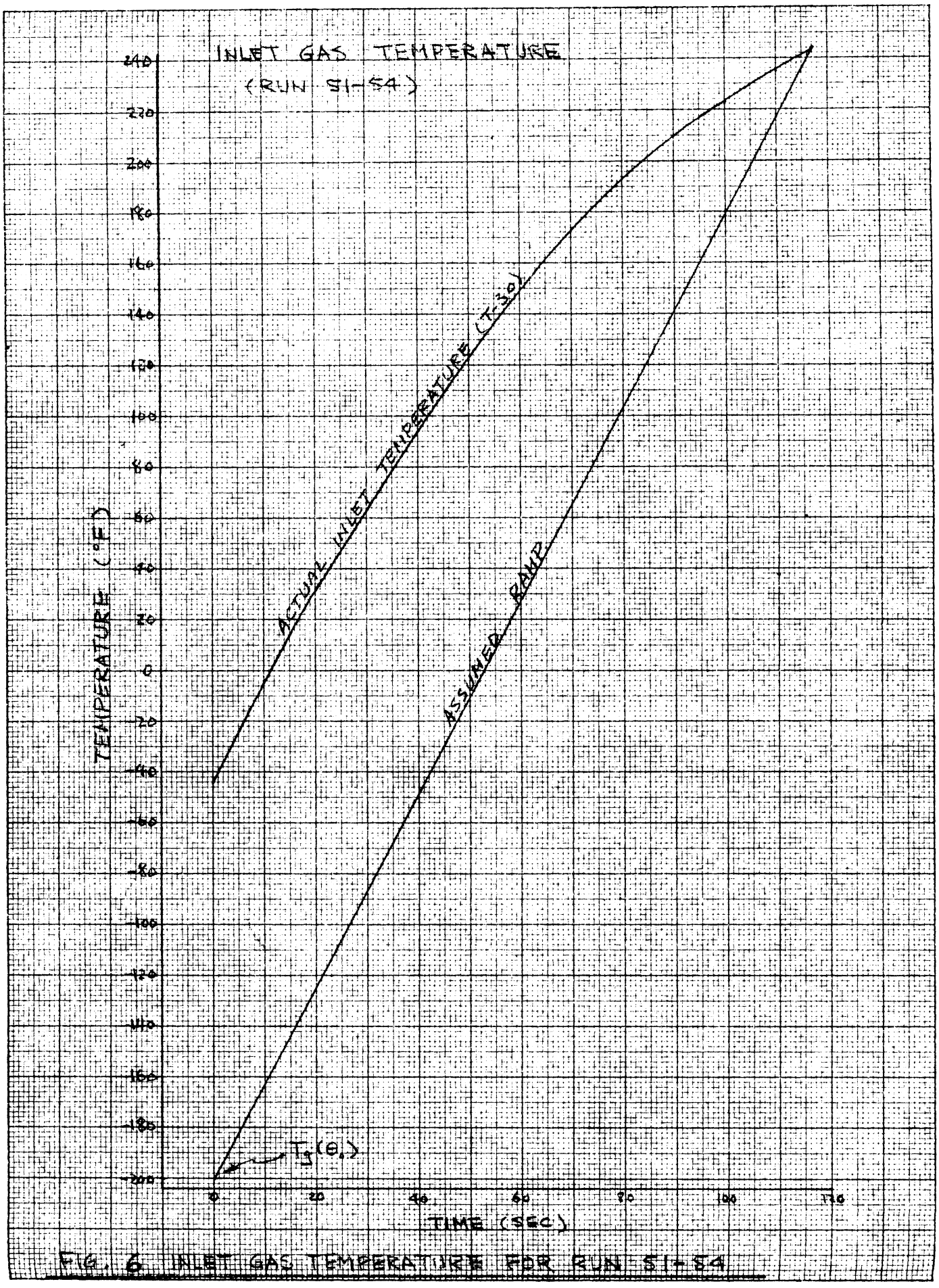

FIG. 6 INLET GAS TEMPERATURE FOR RUN 51-54

MEAN CROSS-SECTIONAL TEMPERATURE VS. DISTANCE FROM INITIAL INTERFACE
RUN 5144 (NASA)
$T_g(\theta_0) = 300°R$
● NASA AVERAGE MEASURED TEMPERATURE
$h_g = 5 \frac{BTU}{HR\ FT^2\ °R}$
$h_s = 3 \frac{BTU}{HR\ FT^2\ °R}$

PREDICTED

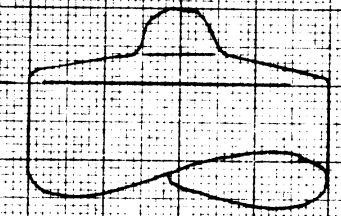

MEAN CROSS-SECTIONAL TEMPERATURE (°R) OF SECONDARY MATERIAL MEASURED FROM INITIAL INTERFACE

0 100 200 300 400 500 600 700

0 5 10 15 20 25 30 35 40

DISTANCE FROM INITIAL INTERFACE (x=0.0) FEET

ARC 6-21-62

MEAN CROSS-SECTIONAL TEMPERATURE V.S DISTANCE FROM INITIAL INTERFACE
RUN 51-44 (NASA)
$T_g(0) = 260\,°R$
⊙ - NASA AVERAGED MEASURED TEMPERATURE
$\bar{h}_g = 5 \frac{BTU}{HR\,FT^2\,°R}$
$\bar{h}_s = 3 \frac{BTU}{HR\,FT^2\,°R}$

PREDICTED

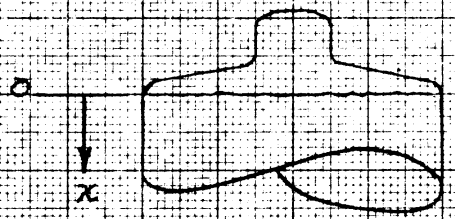

EXHIBIT MEAN CROSS-SECTIONAL TEMPERATURE V.S DISTANCE FROM INITIAL INTERFACE

MEAN CROSS-SECTIONAL TEMPERATURE °R

700
600
500
400
300
200
100
0

0 5 10 15 20 25 30 35 40

DISTANCE FROM INITIAL INTERFACE (X=0.0) FEET

ABC
6-22-62

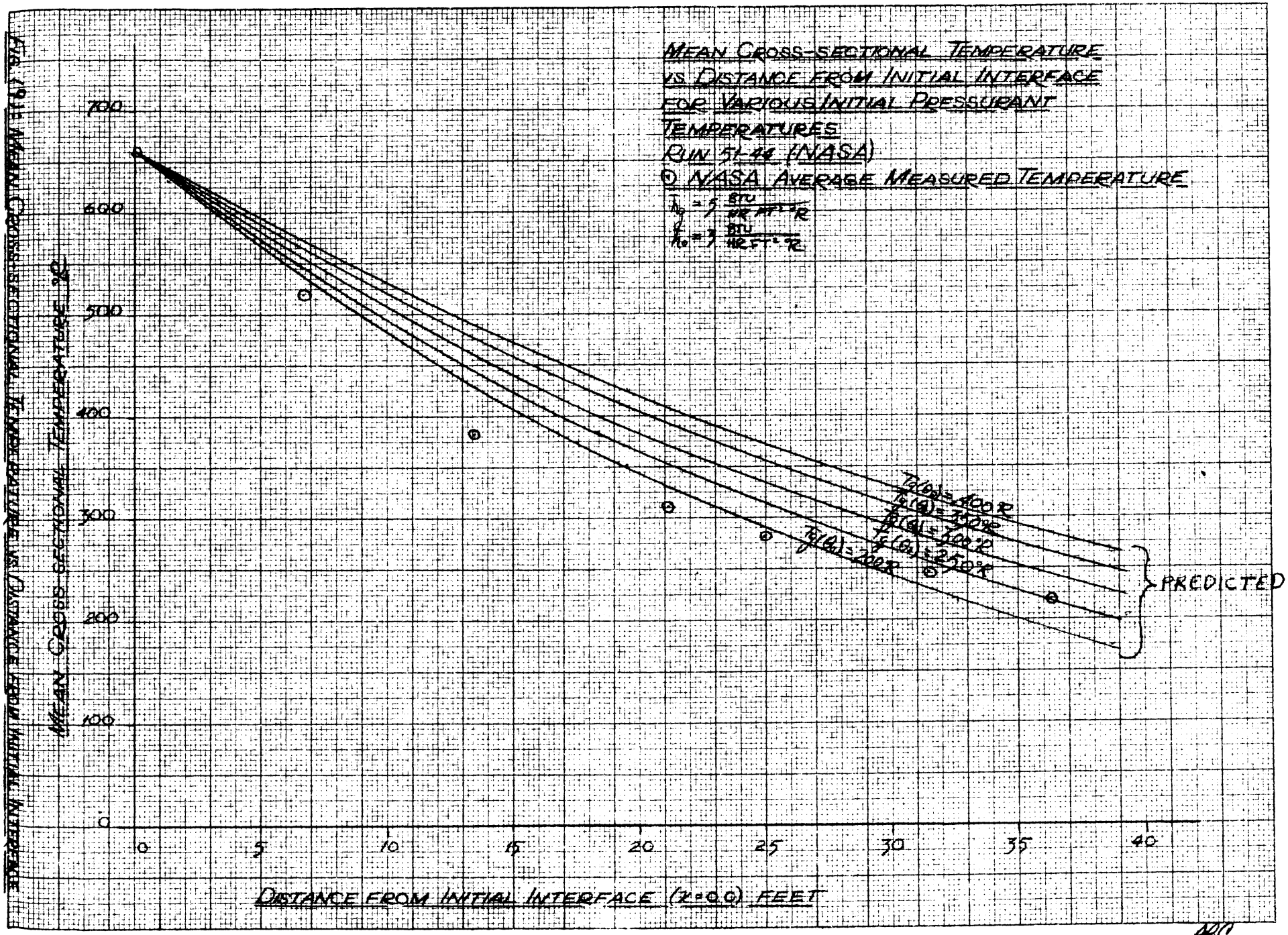
MEAN CROSS-SECTIONAL TEMPERATURE VS DISTANCE FROM INITIAL INTERFACE FOR VARIOUS INITIAL PROPELLANT TEMPERATURES
RUN 51-44 (NASA)
⊙ NASA AVERAGE MEASURED TEMPERATURE
$h_o = 5 \frac{BTU}{HR\,FT^2\,°R}$
$h_o = 7 \frac{BTU}{HR\,FT^2\,°R}$
$T_P(0) = 460°R$
$T_P(0) = 360°R$
$T_P(0) = 260°R$
$T_P(0) = 210°R$
$T_P(0) = 160°R$
PREDICTED
MEAN CROSS-SECTIONAL TEMPERATURE °R (NASA MEASURED TEMPERATURE FROM INITIAL INTERFACE)
700
600
500
400
300
200
100
0
0
5
10
15
20
25
30
35
40
DISTANCE FROM INITIAL INTERFACE (x=0.0) FEET

ABC
6-22-62

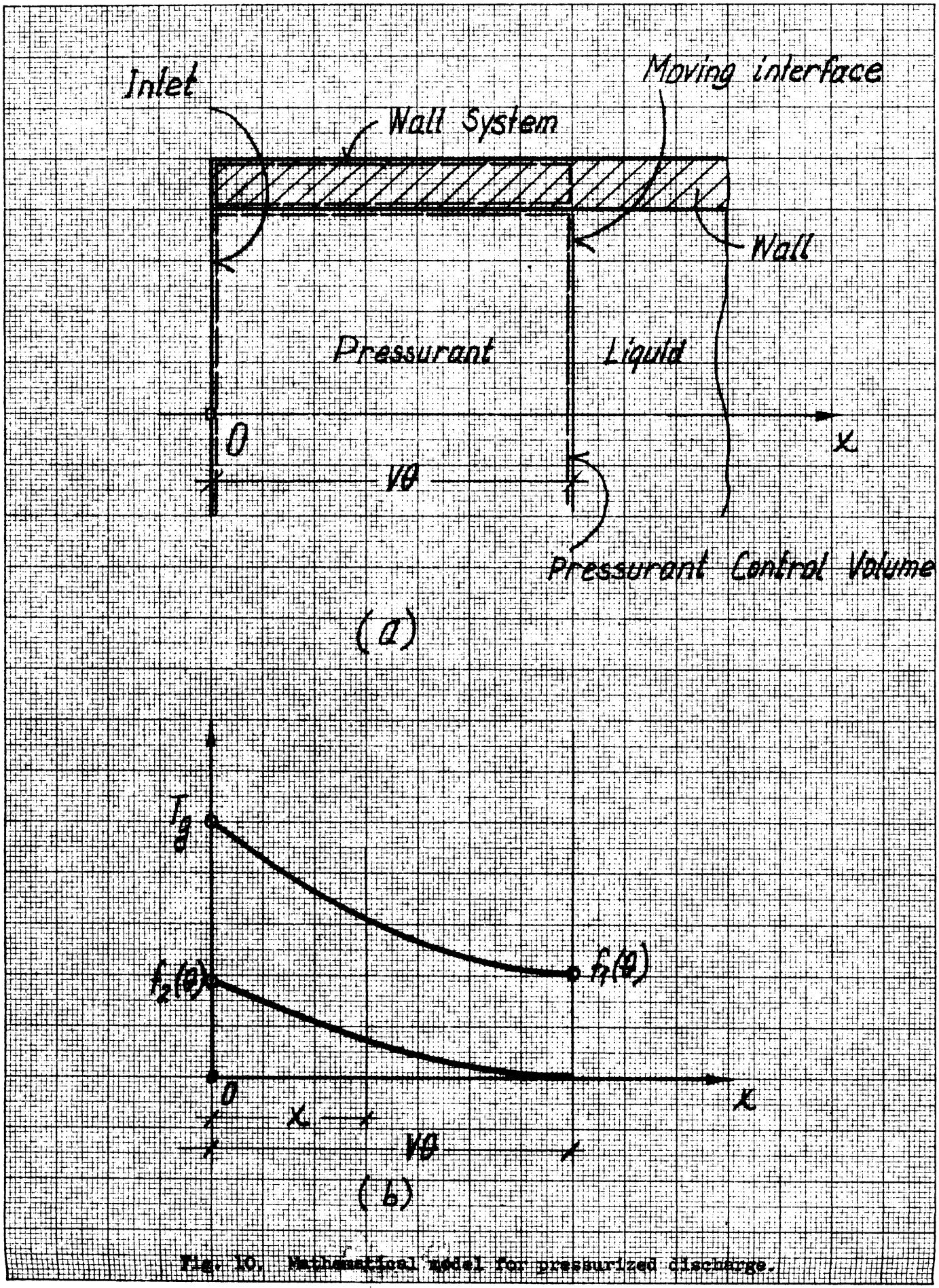

Fig. 10. Mathematical model for pressurized discharge.

a) Wall Energy equation

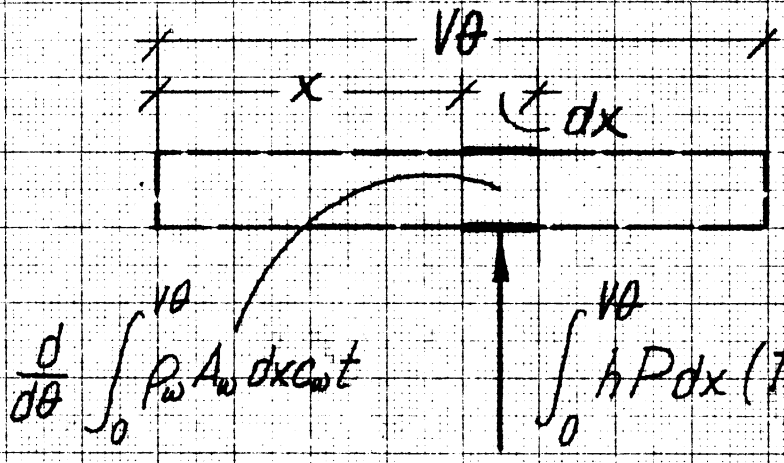

b) Pressurant Energy equation

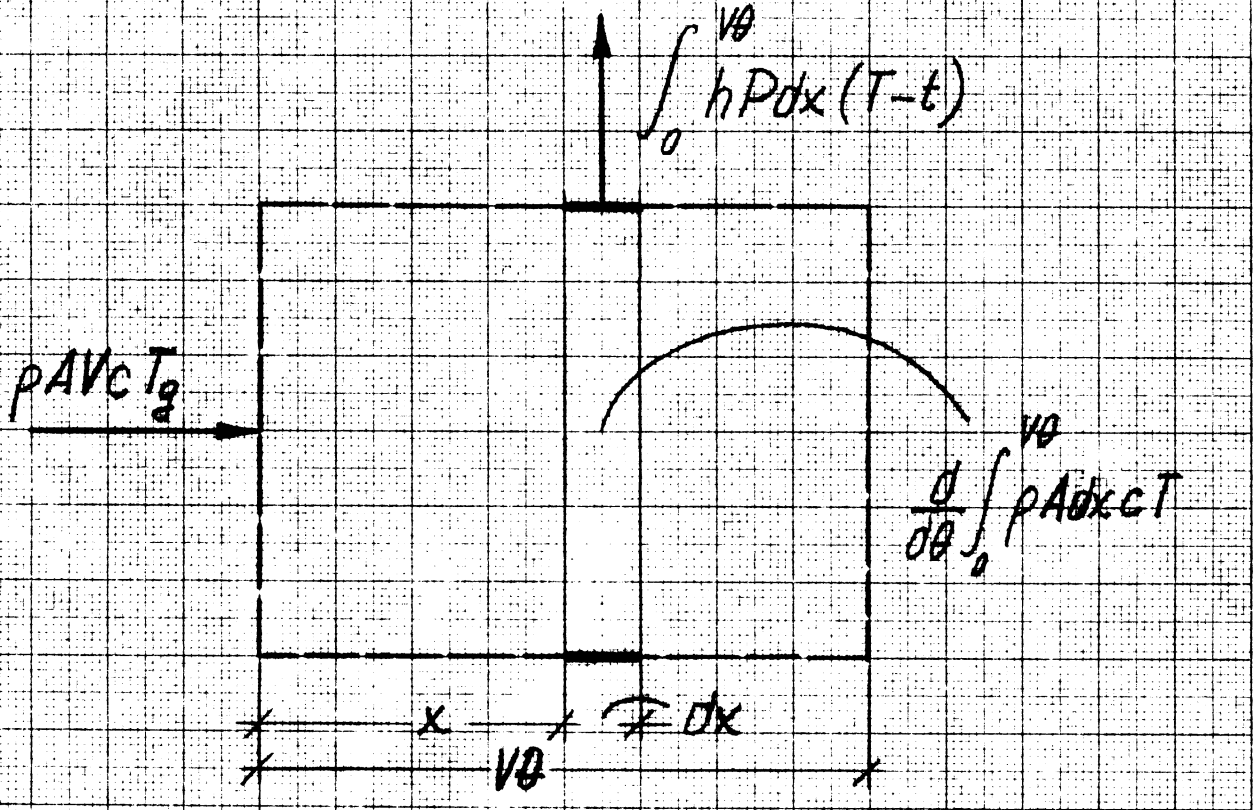

Fig. 11. Schematic representation of wall and pressurant energy equations.

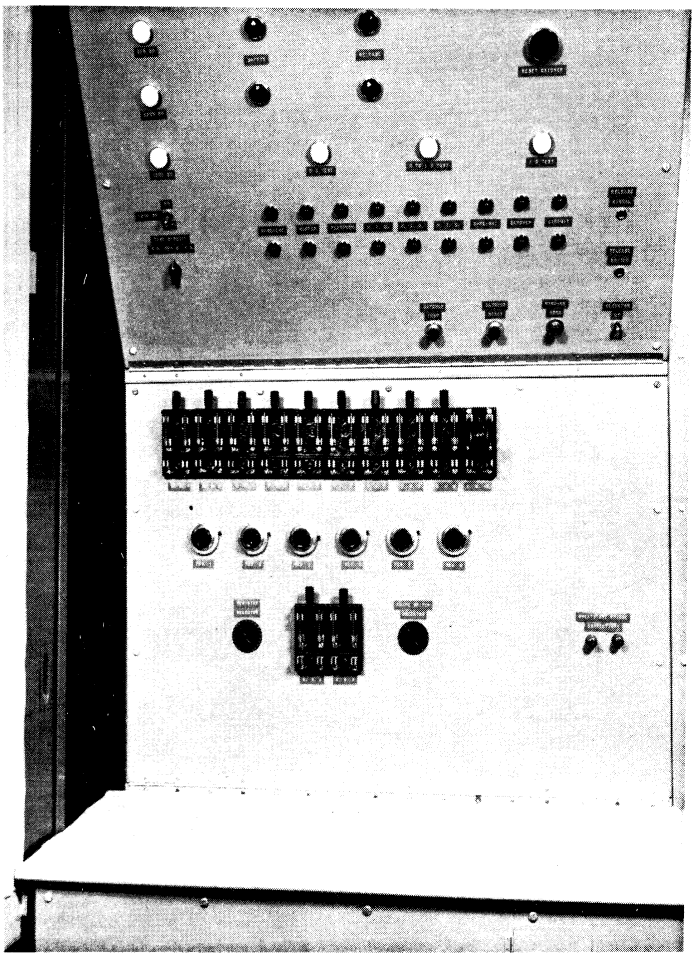

Fig. 12. Reduced gravity test facility control panel.

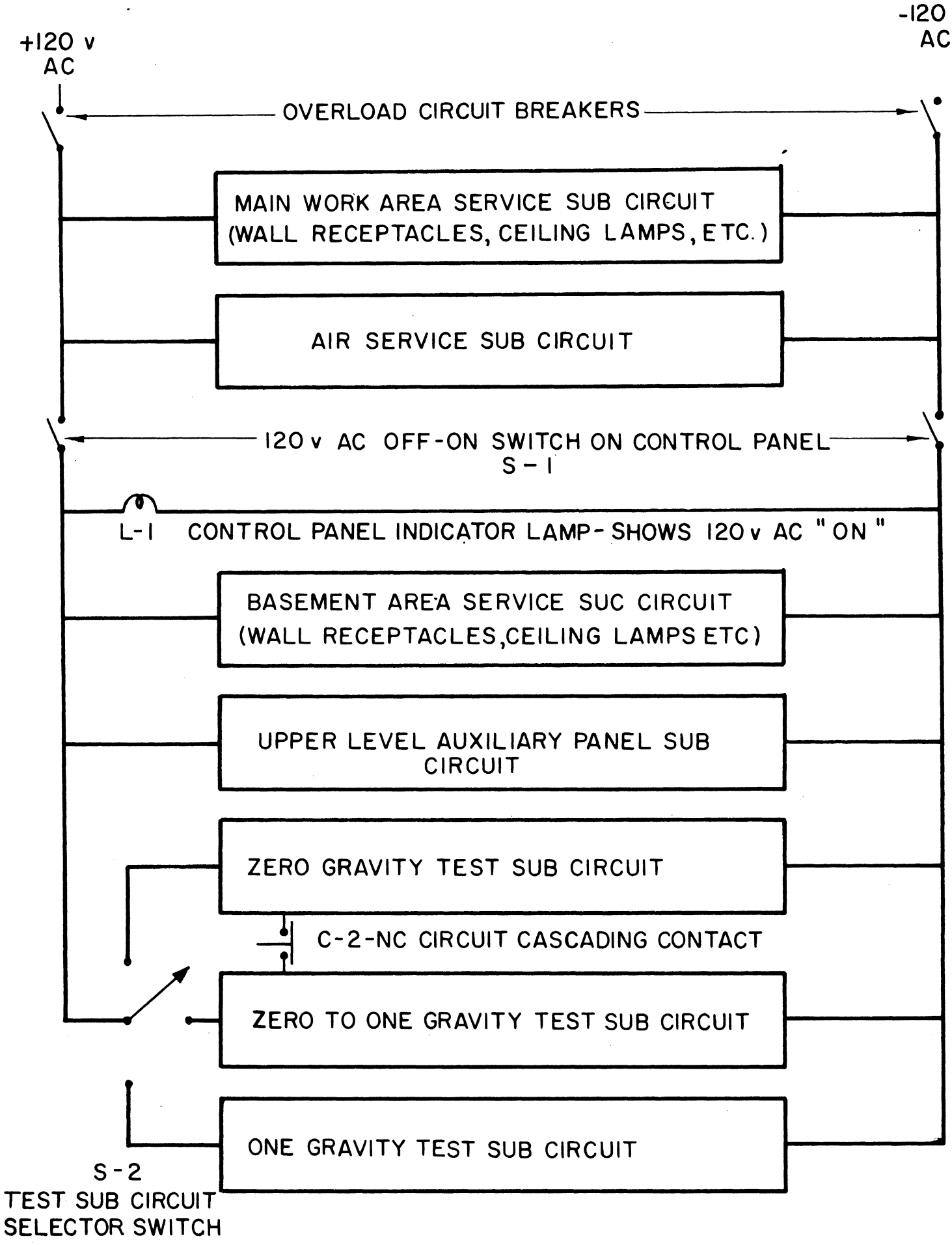

Fig. 13: Reduced gravity electrical circuit. 120 VAC supply.

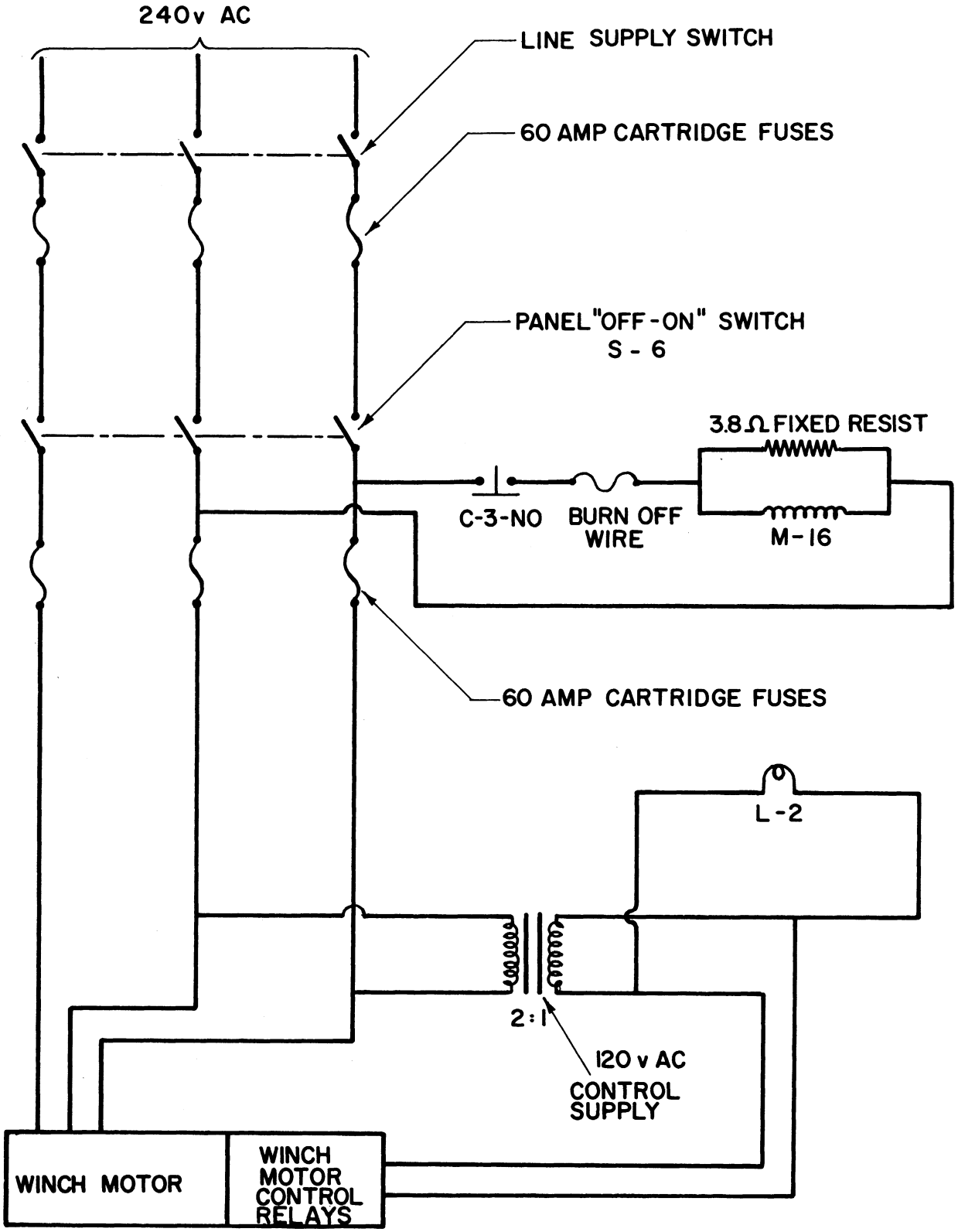

Fig. 14. Reduced gravity electrical circuit. 240 VAC supply.

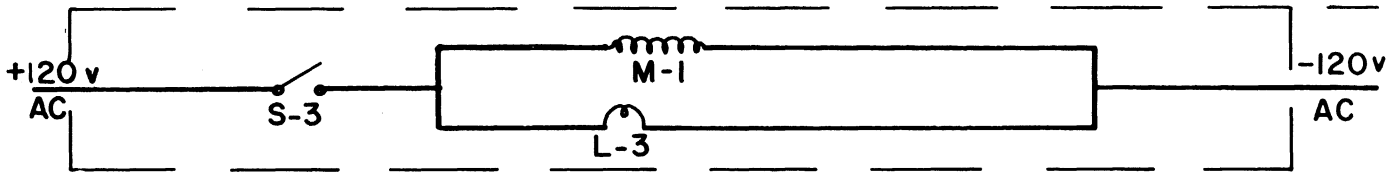

AIR SERVICE SUB CIRCUIT

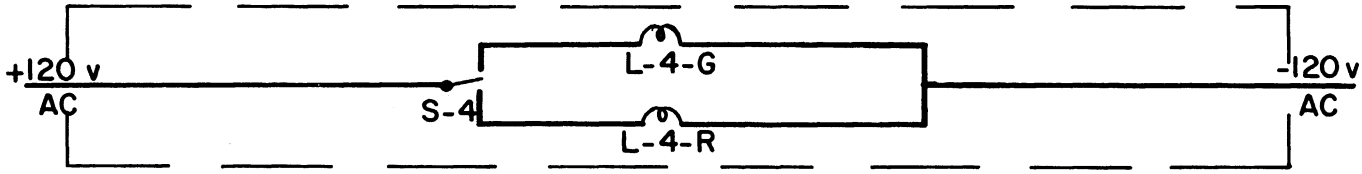

UPPER LEVEL AUXILIARY PANEL SUB CIRCUIT

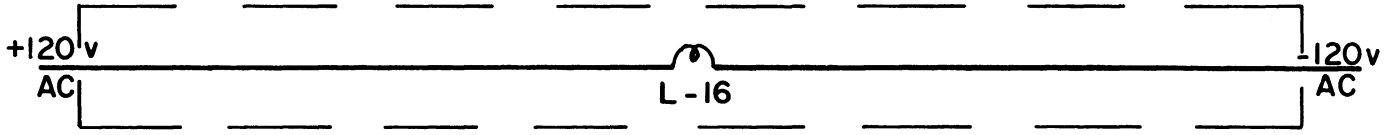

ONE GRAVITY TEST SUB CIRCUIT

Fig. 15. Reduced gravity electrical circuit. Sub-circuits.

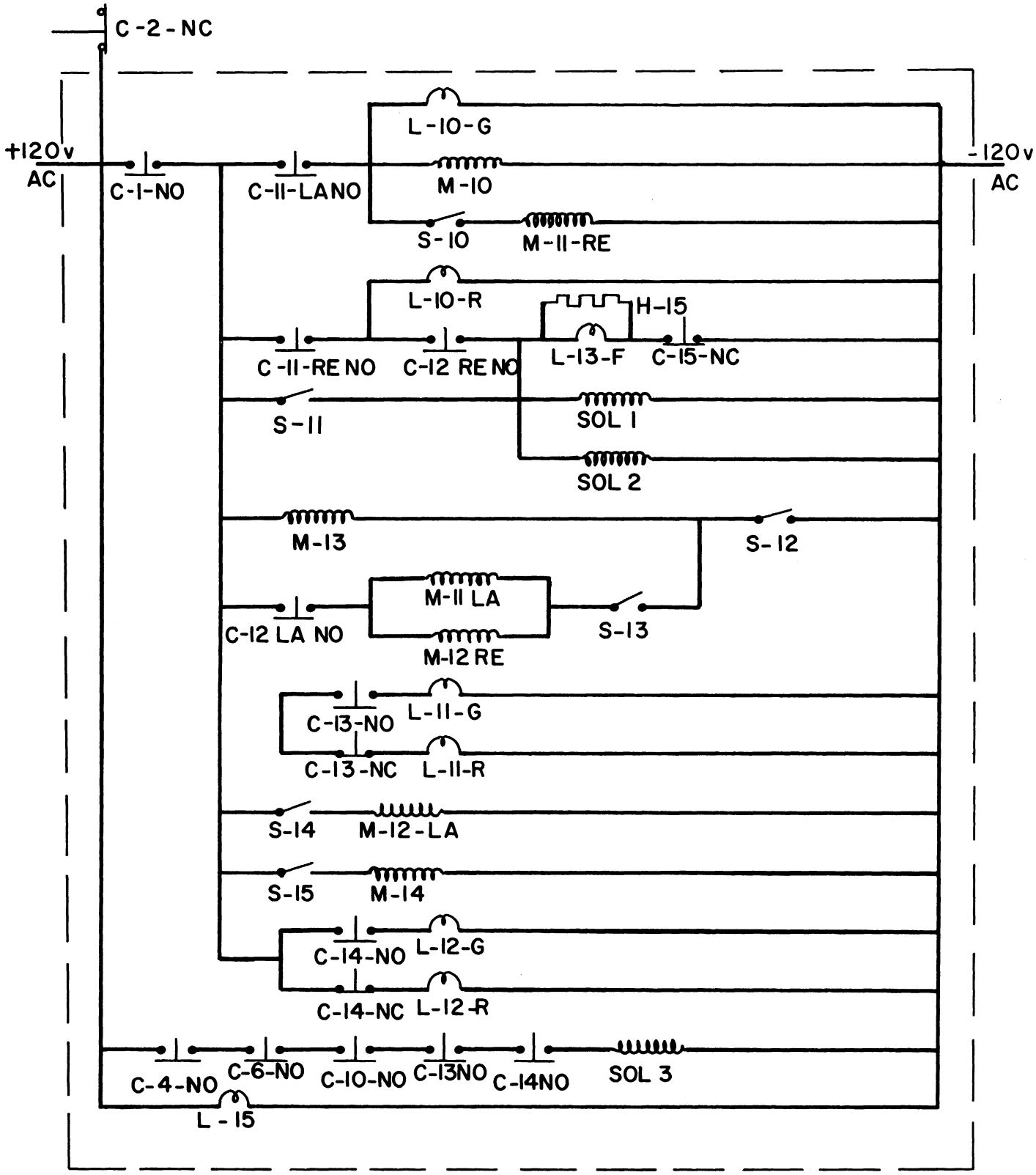

Fig. 16. Reduced gravity electrical circuit.
Fractional gravity sub-circuit.

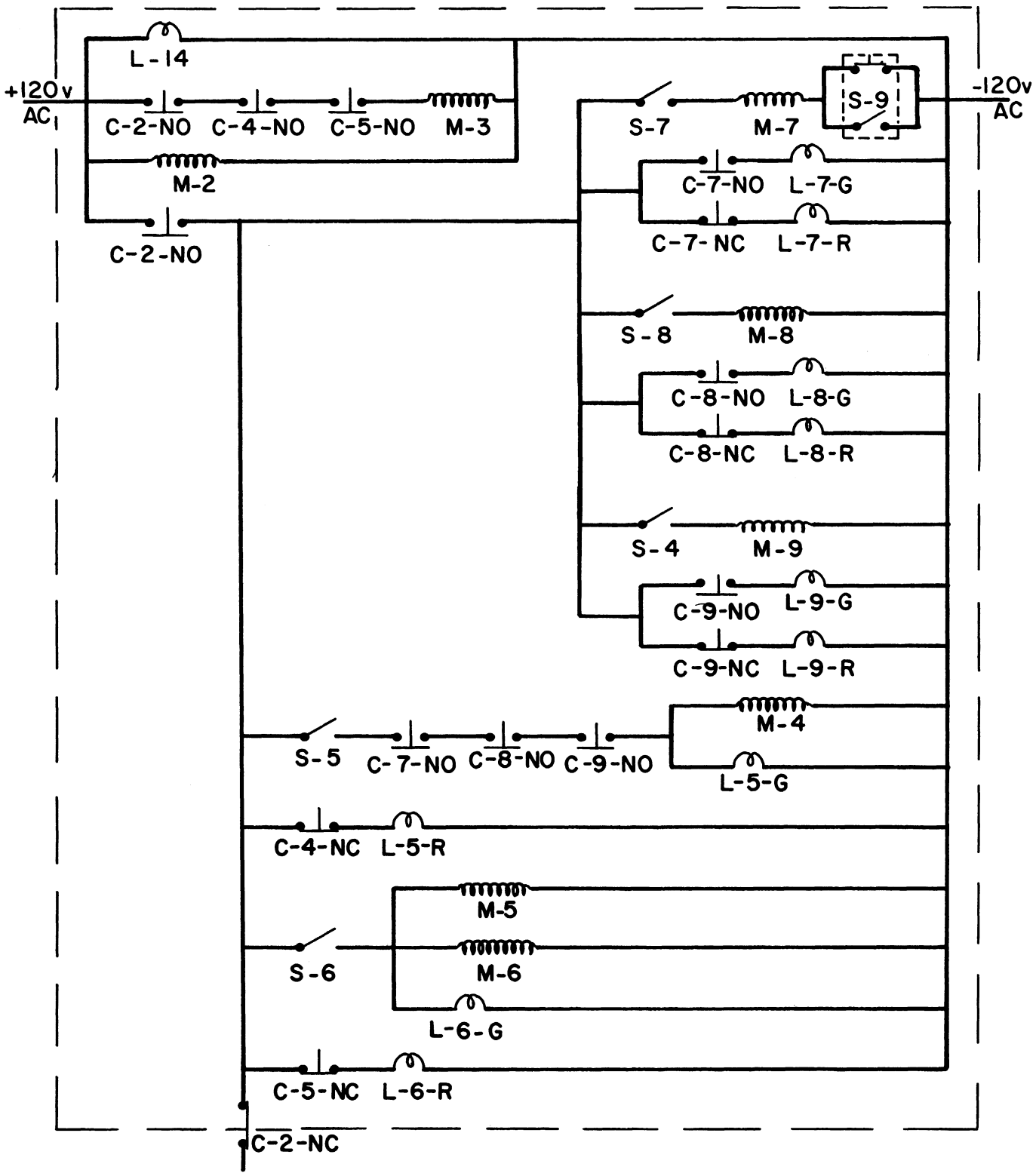

Fig. 17. Reduced gravity electrical circuit.
Free fall sub-circuit.

Relays

Relay	Name	Contacts	Function
M-1	Air Service	C-1-NO	Interlock for air with fractional gravity
M-2	Cascade	C-2-NO	Energizes free fall circuit
		C-2-No	" " " "
		C-2-NC	" fractional gravity circuit
M-3	Burn Wire	C-3-NO	Close contact to release test package-free fall
M-4	Safety Interlock	C-4-NO	In series with M-3
		C-4-NC	Actuates L-5-R
		C-4-No	In series with Sol 3
M-5	Safety Hook	C-5-NO	In series with M-3
		C-5-NC	Actuates L-6-R
M-6	Safety Hook	C-6-NO	In series with Sol 3
M-7	Enclosure Door	C-7-NO	In series with M-4
		C-7-NO	Actuates L-7-G
		C-7-NC	" L-7-R
M-8	Buffer Piston	C-8-NO	In series with M-4
		C-8-NO	Actuates L-8-G
		C-8-NC	" L-8-R
M-9	Upper Level Ready	C-9-NO	In series with M-4
		C-9-NO	Actuates L-9-G
		C-9-NC	" L-9-R
M-10	Counterweight Trapdoor Ready	C-10-NO	In series with Sol 3
M-11-LA	Trapdoor Action	C-11-LA-NO	Actuates M-10
-RE	Latching	C-11-RE-NO	Reset for M-10
M-12-LA	Trapdoor Action	C-12-LA-NO	In series with M-11 LA
-RE	Latching	C-12-RE-NO	In series with Sol 1 and 2

Fig. 18. Reduced Gravity Electrical Circuit—Nomenclature.

Relay	Name	Contacts	Function
M-13	Counterweight Trapdoor Ready	C-13-NO	In series with Sol 3
		C-13-NO	Actuates L-11-G
		C-13-NC	" L-11-R
M-14	Counterweight Ready	C-14-NO	In series with Sol 3
		C-14-NO	Actuates L-12-G
		C-14-NC	" L-12-R
M-15-H	Trapdoor Extended Indicator	C-15-NC	Actuates L-13-F
M-16	Burn Wire Release	C-16-NO	Provides release signal

Solenoids

No.	Function
Sol 1	Trapdoor Air Action Valve
Sol 2	" " Exhaust "
Sol 3	Counterweight Release

Switches

No.	Type	Function
S-1	DPST	120 VAC Supply
S-2	SP3T	Sub circuit selector
S-3	SPST	Air pressure switch
S-4	DPDT	Upper level ready
S-5	SPST	Remote test package release
S-6	SPST	Actuated by safety hook
S-7	SPST	" " enclosure door

Fig. 18. Continued.

Switches

No.	Type	Function
S-8	SPST	Actuated by buffer piston
S-9	DPDT	Lower Level auxiliary release
S-10	SPST	Trapdoor trip
S-11	SPST	Trapdoor test
S-12	SPST	Trapdoor ready
S-13	SPST	Trapdoor circuit reset
S-14	SPST	Trapdoor reset
S-15	SPST	Counterweight ready
S-16	TPST	240 VAC Supply

Indicator Lights

No.	Function
L-1	120 VAC ON
L-2	240 VAC ON
L-3	Air Supply ON
L-4-G	Upper Level Ready
-R	" " Not Ready
L-5-G	Release Circuit Closed
-R	" " Opened
L-6-G	Safety Hook Withdrawn
-R	" " Not Withdrawn
L-7-G	Lower Enclosure door closed
-R	" " " open

Fig. 18. Continued.

L-8-G	Buffer Piston Ready
-R	" " Not Ready
L-9-G	Upper Level Ready
-R	" " Not Ready
L-10-G	Trapdoor Circuit Ready
-R	" " Not Ready
L-11-G	Trapdoor Ready
-R	" Not Ready
L-12-G	Counterweight Ready
-R	" Not Ready
L-13-F	Warning - Trapdoor not reset
L-14	1 g operation
L-15	Reduced gravity operation
L-16	Free fall operation

Fig. 18. Concluded

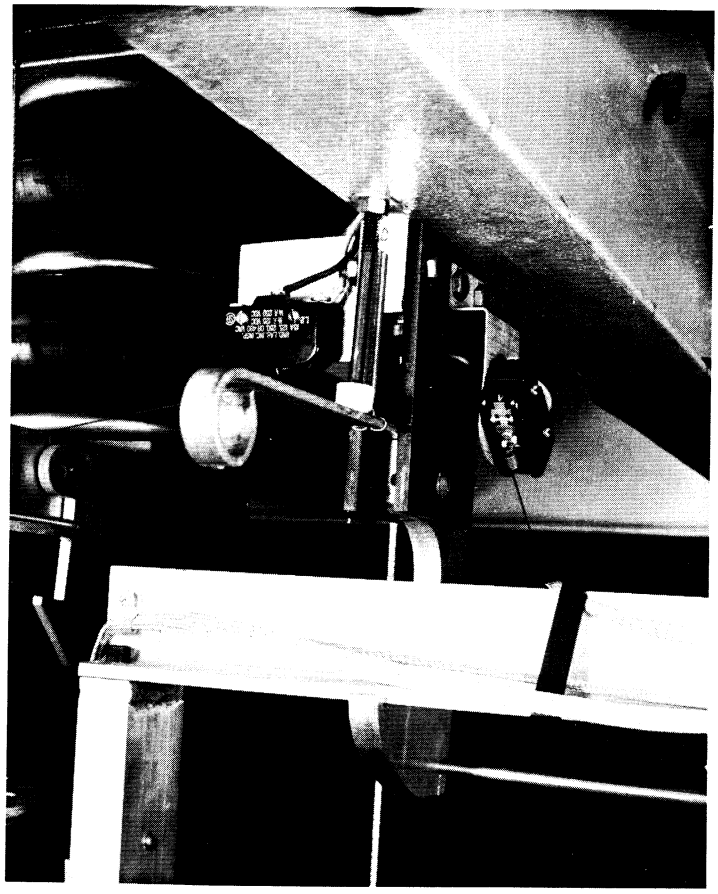

Fig. 19. Closeup view of safety hook.

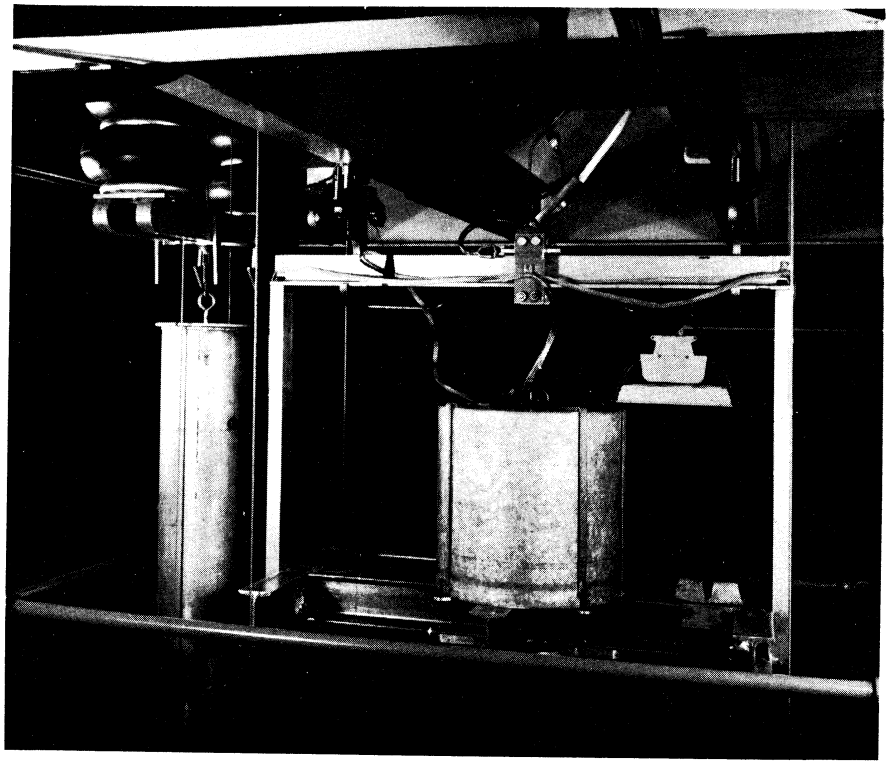

Fig. 20. View of test platform and counterweight.

```
                DIMENSION X(100),Y(100),X1(100),Y1(2500 Y1DIM),X2(100),
               1Y2(121,Y2DIM),X3(100),Y3(121,Y3DIM),T(100),TN(100),TA(100)
                INTEGER I,J,K,L,N,R,S,SM
START           READ DATA
                PRINT RESULTS N,DS,RHO,DR,TC,SM,VA,RO,X(1)...X(N),Y(1)...Y(N)
               1,TL
                THROUGH LOOPB  FOR I=3,2,I.G.(N-1)
                THROUGH LOOPC  FOR J=I-2,1,J.G.(I+2)
                X1(J)=X(J)
LOOPC           Y1(J I-2)=Y(J)
                THROUGH LOOPD, FOR K=I-1,1,K.G.(I+2)
                THROUGH LOOPD, FOR J=K,1,J.G.(I+2)
LOOPD           Y1(J,K)=Y1(J,K-1)-Y1(J-1,K-1))/(X1(J)-X1(J-K+I-2))
                A=Y(I)
                B=A+340
                C=A+320
                D=A+300
                F=A+280.
                CP=0.0406+4.1E-4*B-1.625E-6*B*C*1.041E-8*B*C*D-4.145E-10*B*C
               1*D*F+9.0925F-12*B*C*D*F*(A+260.)
                CQ=RHO*DR*DR*3600./(TC*DS)
                M=CP*CQ
                P=(X1(I+1)-X1(I-1))/DS
                THROUGH LOOPB FOR L=1.1,L.G.P
                WHENEVER I.G.3 .OR.L.G.1,TRANSFER TO PSI
                THROUGH LOOPE, FOR S=1,1,S.G.SM
LOOPE           T(S)=Y1(2,1)
PSI             TI=X1(I-1)+L*DS
                T(1)=Y1(I-2,I-2)
                Z=1.0
                THROUGH LOOPF FOR J=(I-1),1,J.G. (I+2)
                Z=Z*(TI-X1(J-1))
LOOPF           T(1)=T(1)+Z*Y1(J,J)
                THROUGH LOOPG FOR S=1,1,S.G.SM
                WHENEVER S.E.1
                TN(1)=T(1)
                OR WHENEVER S.L. SM
                DRR=DR/(RO-(S-1)*DR)
                TN(S)=(T(S+1)*(1.-DRR)+T(S-1)*(1.+DRR)+(M-2.)(T(S))/M
                OTHERWISE
                TN(S)=(6.*T(S-1)+(M-6.)*T(S))/M
                END OF CONDITIONAL
                WHENEVER .ABS.(TI-(X1(I)-2.*DS)).L.0.00010
                Y2(S,1)=TN(S)
                X2(1)=TI
                R=1
```

Fig. 22. Digital Computer Program.

```
                OR WHENEVER .ABS.(TI-(X1(I)-DS)).L.0.00010
                Y2(S,2)=TN(S)
                X2(2)=TI
                R=2
                OR WHENEVER . ABS. (TI-X1(I)).L.0.00010
                Y2(S,3)=TN(S)
                X2(3)=TI
                R=3
                OR WHENEVER .ABS.(TI-(X1(I)+DS)).L.0.00010
                Y2(S,4)=TN(S)
                X2(4)=TI
                R=4
                OR WHENEVER .ABS.(TI=(X1(I)+2.*DS)).L.0.00010
                Y2(S,5)=TN(S)
                X2(5)=TI
                R=5
                TD=Y2(1,3)-TL
LOOPG           END OF CONDITIONAL
                THROUGH LOOPH,FOR S=1,1,S.G.SM
LOOPH           T(S)=TN(S)
                WHENEVER .ABS.(TI-(X1(I)+2.*DS)).L.0.00010
                THROUGH LOOPL,FOR R=1,1,R.G.5
                SUM=((SM-1.).P.2*Y2(1,R))/2.
                THROUGH LOOPJ, FOR S=2,1,S.E.SM
LOOPJ           SUM=SUM+((SM=S).P.2)*Y2(S,R)
                TA(R)=3.*SUM/((SM-1.).P.3)
                X3(R)=X2(R)
LOOPL           Y3(R,1)=TA(R)
                THROUGH LOOPK, FOR K=2,1,K.G.5
                THROUGH LOOPK, FOR J=K,1,J.G.5
LOOPK           Y3(J,K)=(Y3(J,K-1)-Y3(J-1,K-1))/(X3(J)-X3(J-K+1))
                TG=Y3(2,2)+(2.*X3(3)-X3(1)-X3(2))*Y3(3,3)
               1+(X3(3)-X3(1))*(X3(3)-X3(2))*Y3(4,4)
               2+(X3(3)-X3(1))*(X3(3)-X3(2))*(X3(3)-X3(4))*Y3(5,5)
                Q=RHO*CP*TG*VA*3600.
                VECTOR VALUES Y1DIM = 2,1,50
                VECTOR VALUES Y2DIM = 2,1,11
                VECTOR VALUES Y3DIM = 2,1,11
                PRINT RESULTS X2(3),Y2(1,3),Y2(2,3),Y2(11,3),CP,Q,TD
                END OF CONDITIONAL
LOOPB           CONTINUE
                TRANSFER TO START
                END OF PROGRAM
```

Fig. 22. Concluded.

CP = Specific Heat of Sphere

CQ = $\frac{\rho(\Delta r)^2 \times 3600}{k(\Delta\theta)}$

DR = Δr = Radius Subdivision

DS = $\Delta\theta$ = Computational Time Interval

TC = k = Thermal Conductivity of Sphere

I = Index on Input Data Points

J = Temporary Index on I

K = " " " "

L = Index on P

M = $\frac{(\Delta r)^2}{a(\Delta\theta)}$ (3600)

N = Total No. of Input Data Points

P = No. of Computational Steps in Computation Interval

Q = Heat Flux

R = Index for Temporary Storage

RHO = ρ = Density of Sphere

RO = Outer Sphere Radius

S = Index of shells of Thickness DR in Sphere

SM = Max. no. of Sphere Subdivision

SUM = Subcomputation for Average Sphere Temperature

TA(R) = Average Sphere Temperature

TC = k = Thermal Conductivity of Sphere

TD = Temperature Difference between Sphere Surface and Fluid Saturation

TG = Sphere Average Temperature-Time Gradient

Fig. 23. Notation Used in Digital Computer Program.

TI = Time

TL = Fluid Saturation Temperature

T(S) = Temperature of Shell S of Sphere

TN(S) = Predicted Temperature of Shell S of Sphere

VA = Sphere Volume-Area Ratio

X(I) = Input Data Time

Y(I) = Input Surface Temperatures

X1(I) = Input Data Time in Temporary Storage

Y1(I) = Input Surface Temperatures in Temporary Storage

Y2(S,R) = Temporary Storage of Temperature

X2(R) = " " " Time

Y3(R,1) = Temporary Storage of Temperature

X3(R) = " " " Time

Fig. 23. Concluded

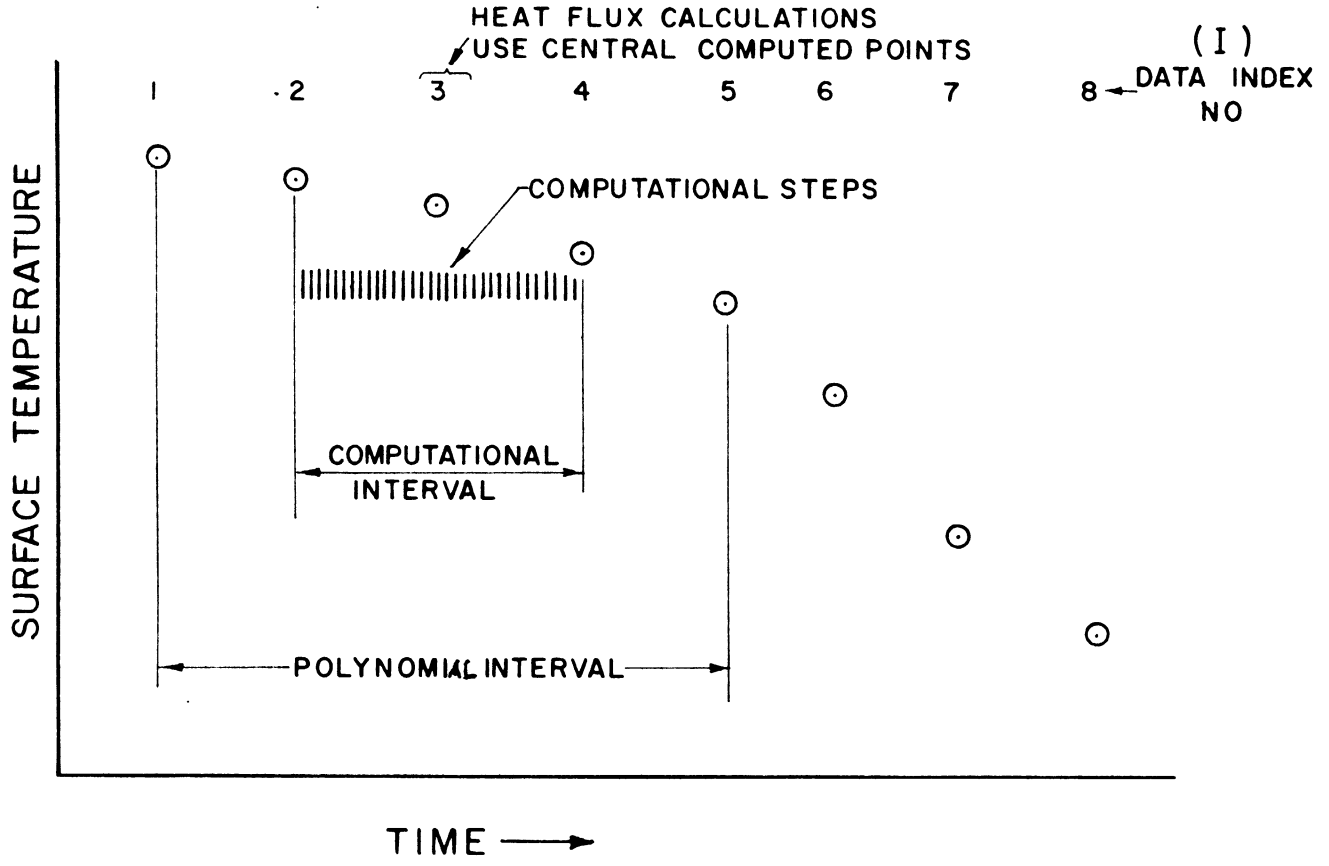

Fig. 24. Computational Procedure for Digital Computer Program.

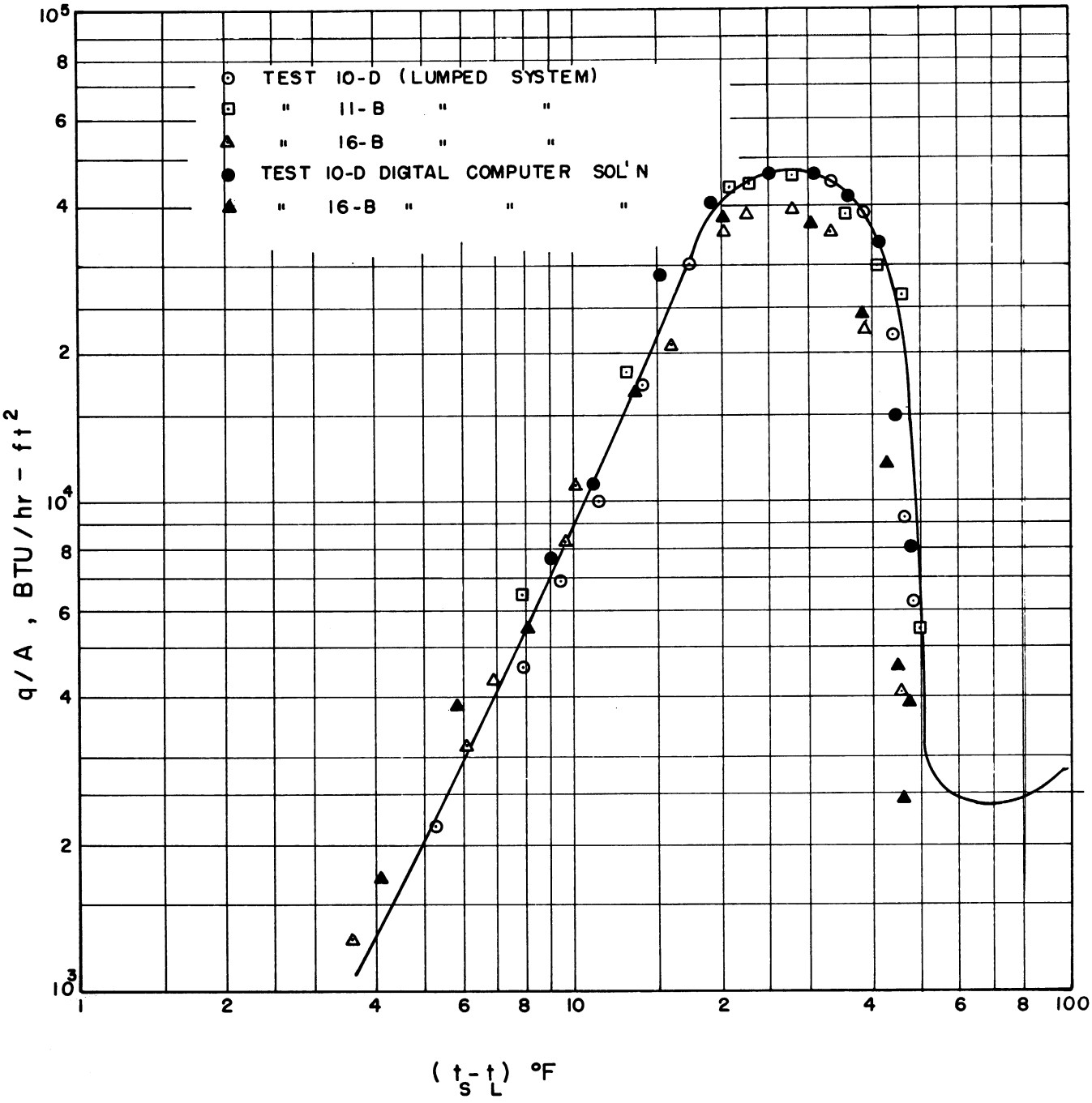

Fig. 25. Comparison between data reduced by hand by Digital Computer.

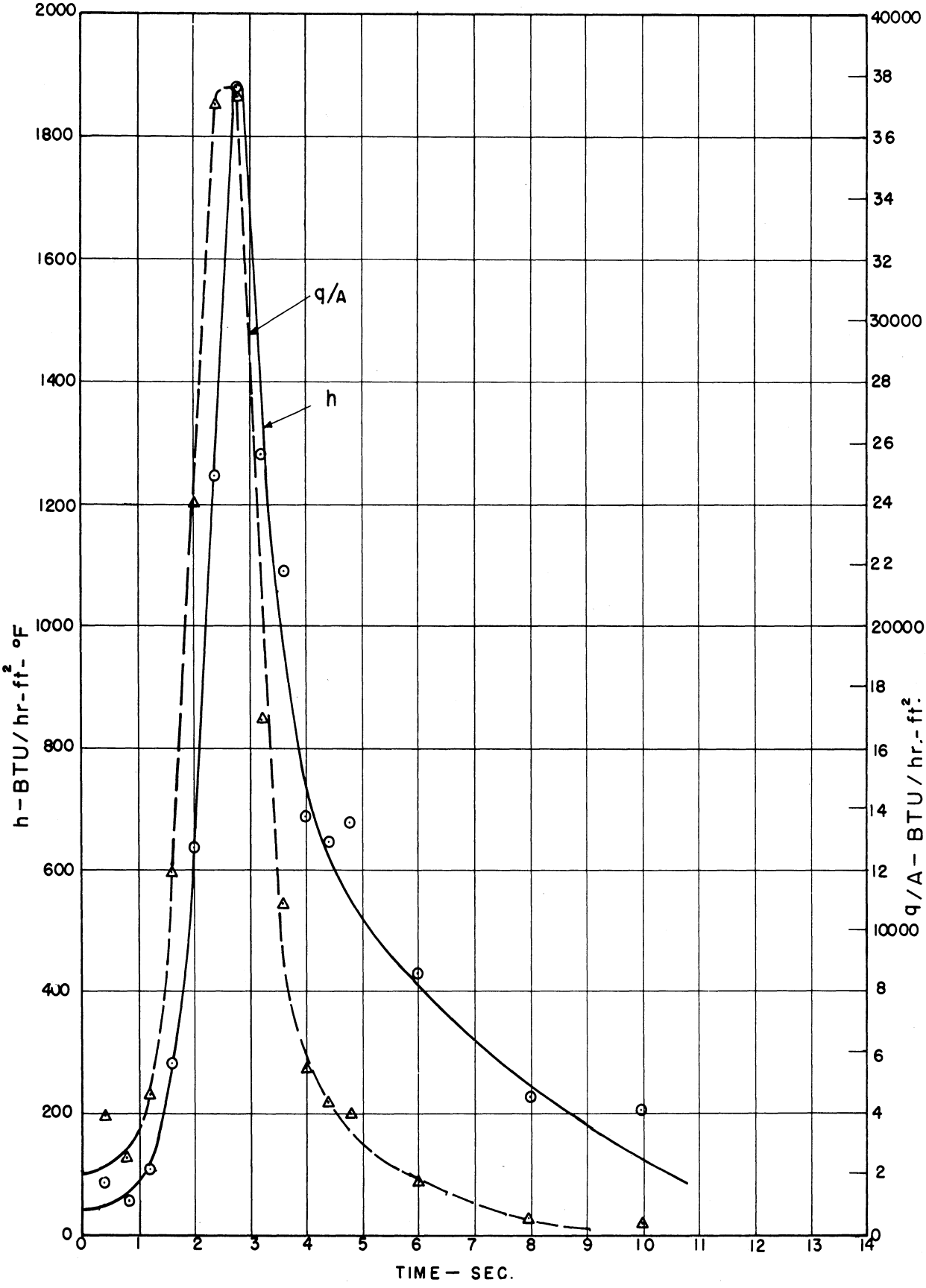

Fig. 26. Variation of heat flux and heat transfer coefficient with time. Test 16-B.

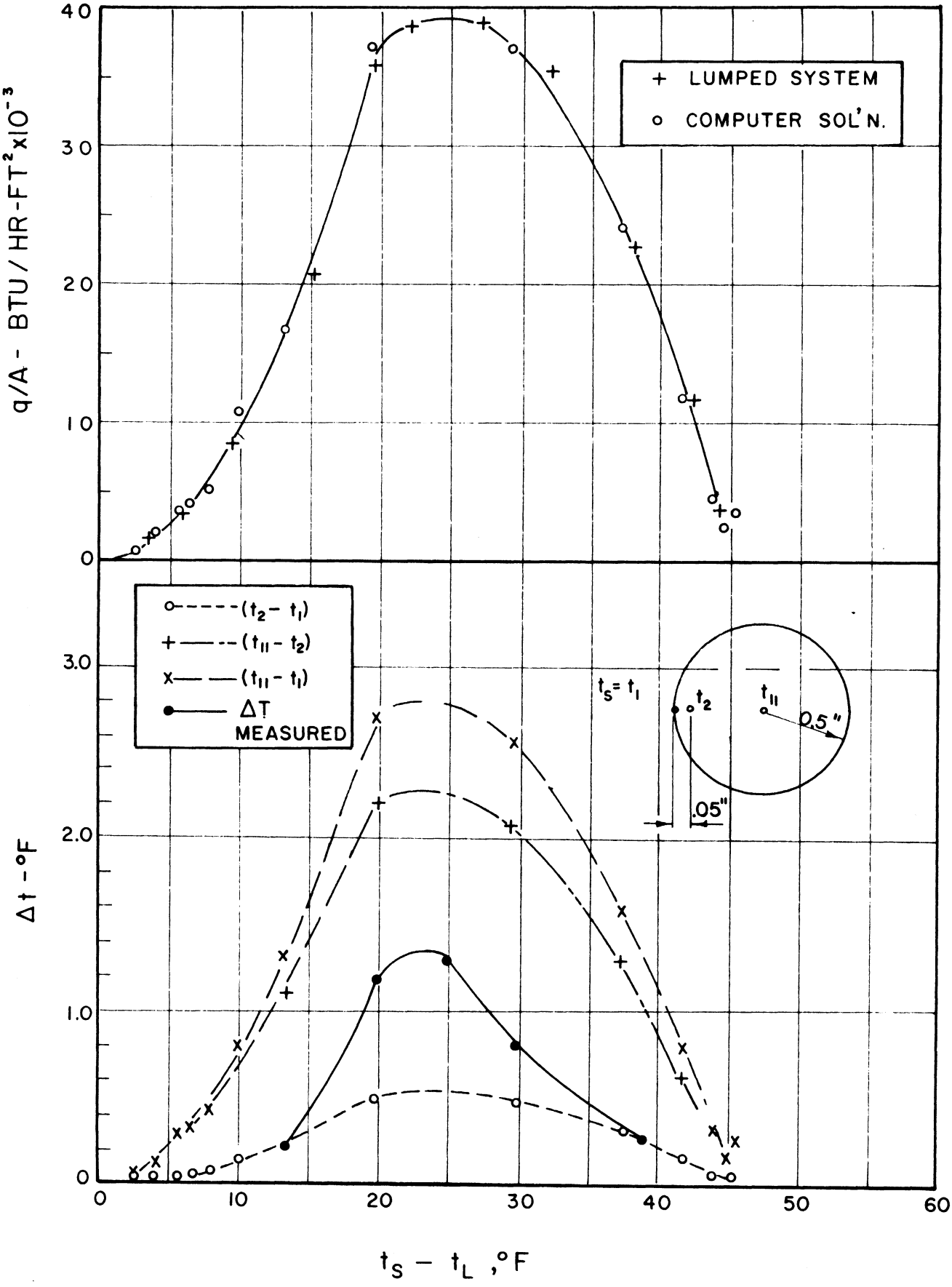

Fig. 27: Comparison of Temperature differences within sphere. Test 16-B.

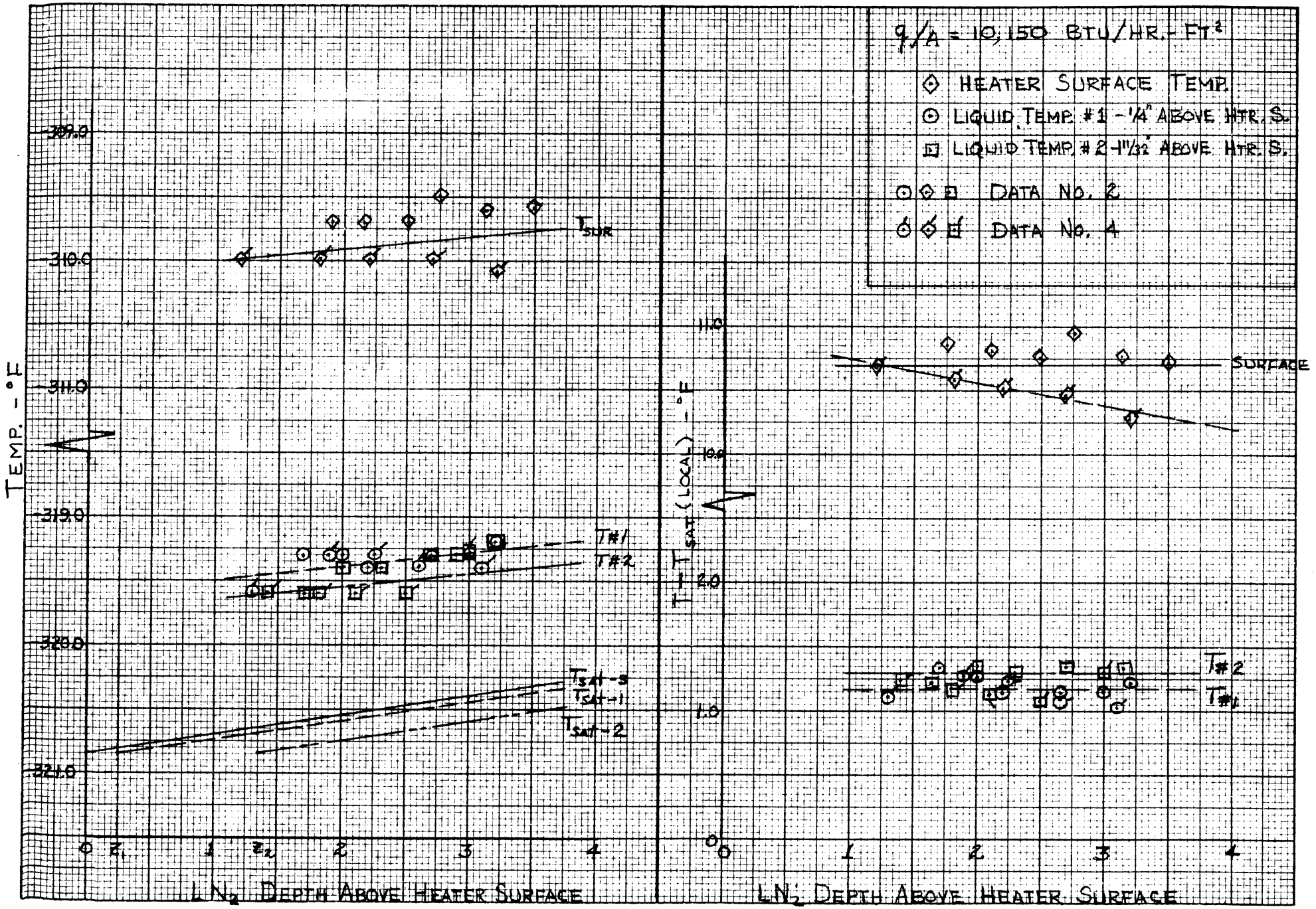

FIGURE 29. INFLUENCE OF LIQUID DEPTH ON TEMPERATURES.
RUN NO. 21 $\alpha/g = 5.6$

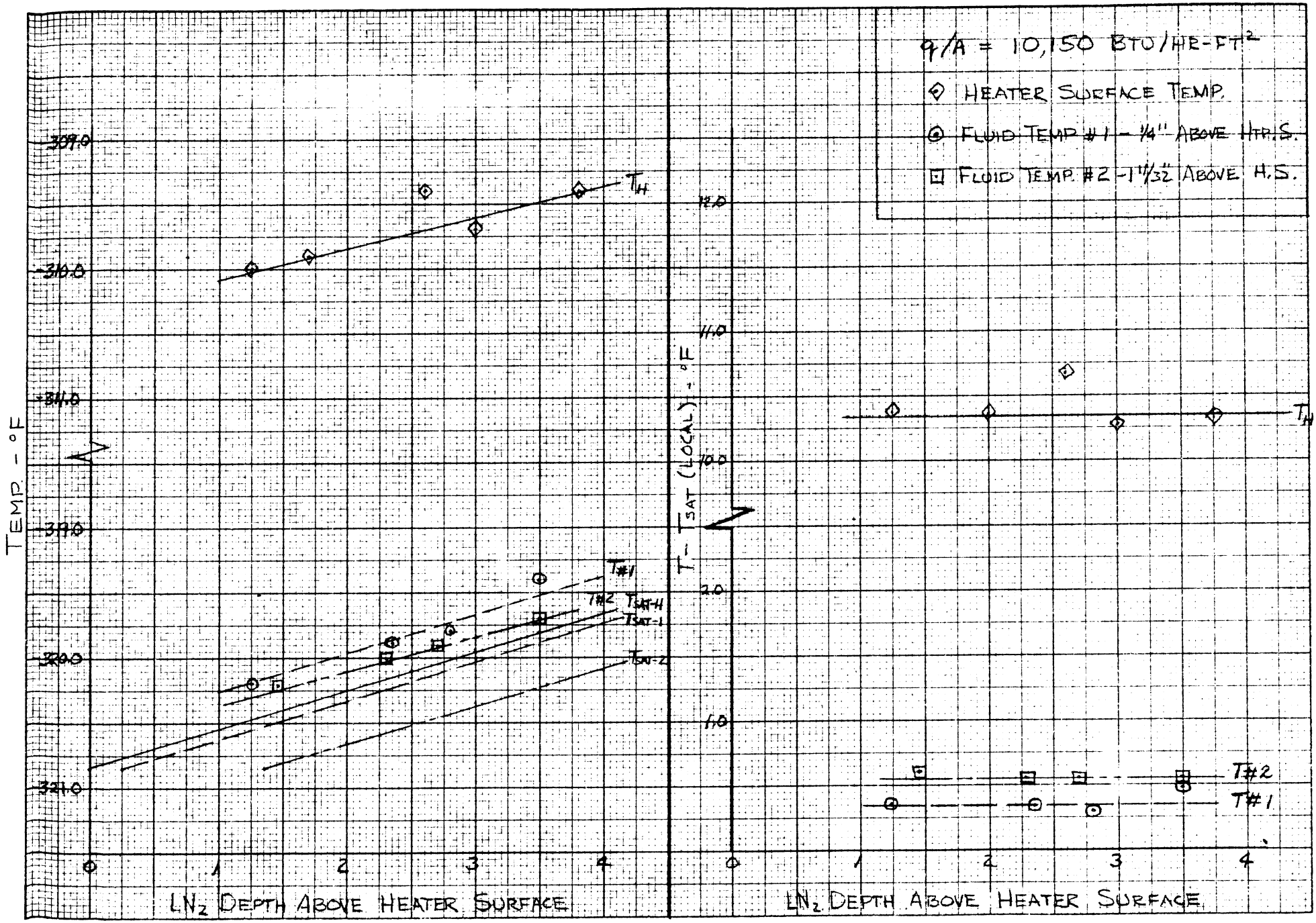

FIGURE 30. INFLUENCE OF LIQUID DEPTH ON TEMPERATURES
RUN NO. 21 $a/g = 10.9$

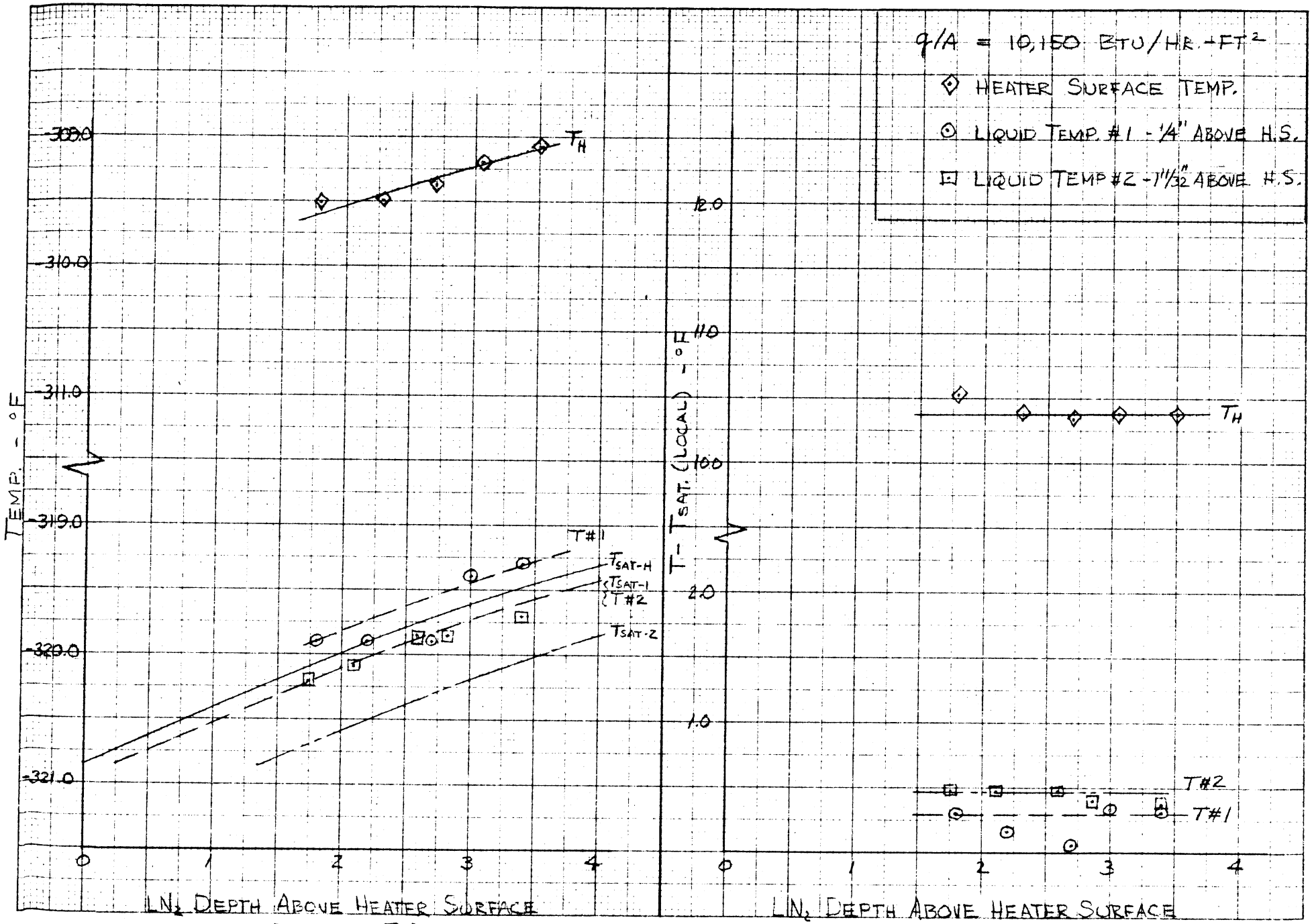

FIGURE 31. INFLUENCE OF LIQUID DEPTH ON TEMPERATURES
RUN NO. 21 a/g = 14.3

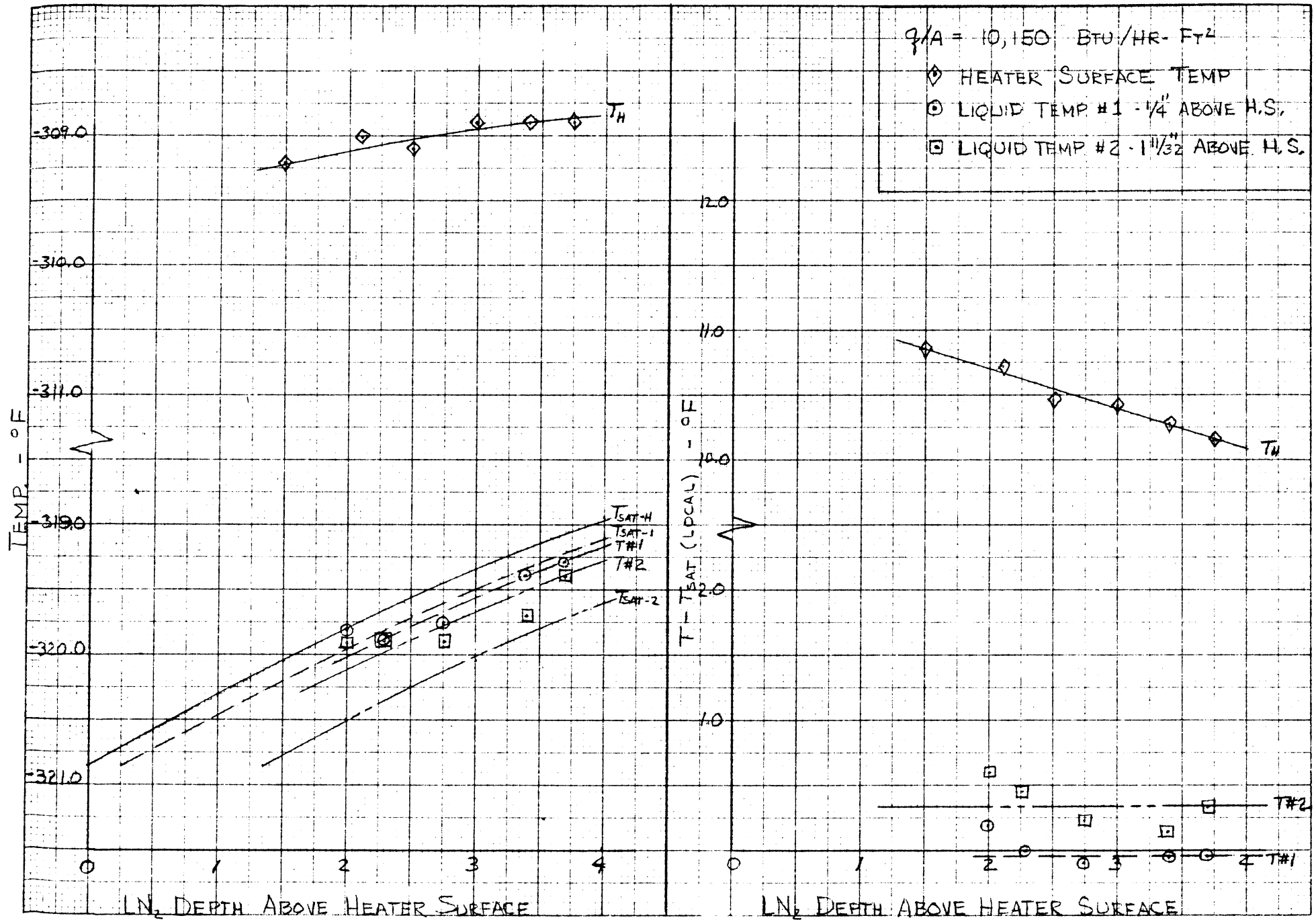

FIGURE 32. INFLUENCE OF LIQUID DEPTH ON TEMPERATURES
RUN NO. 21 a, = 18.3

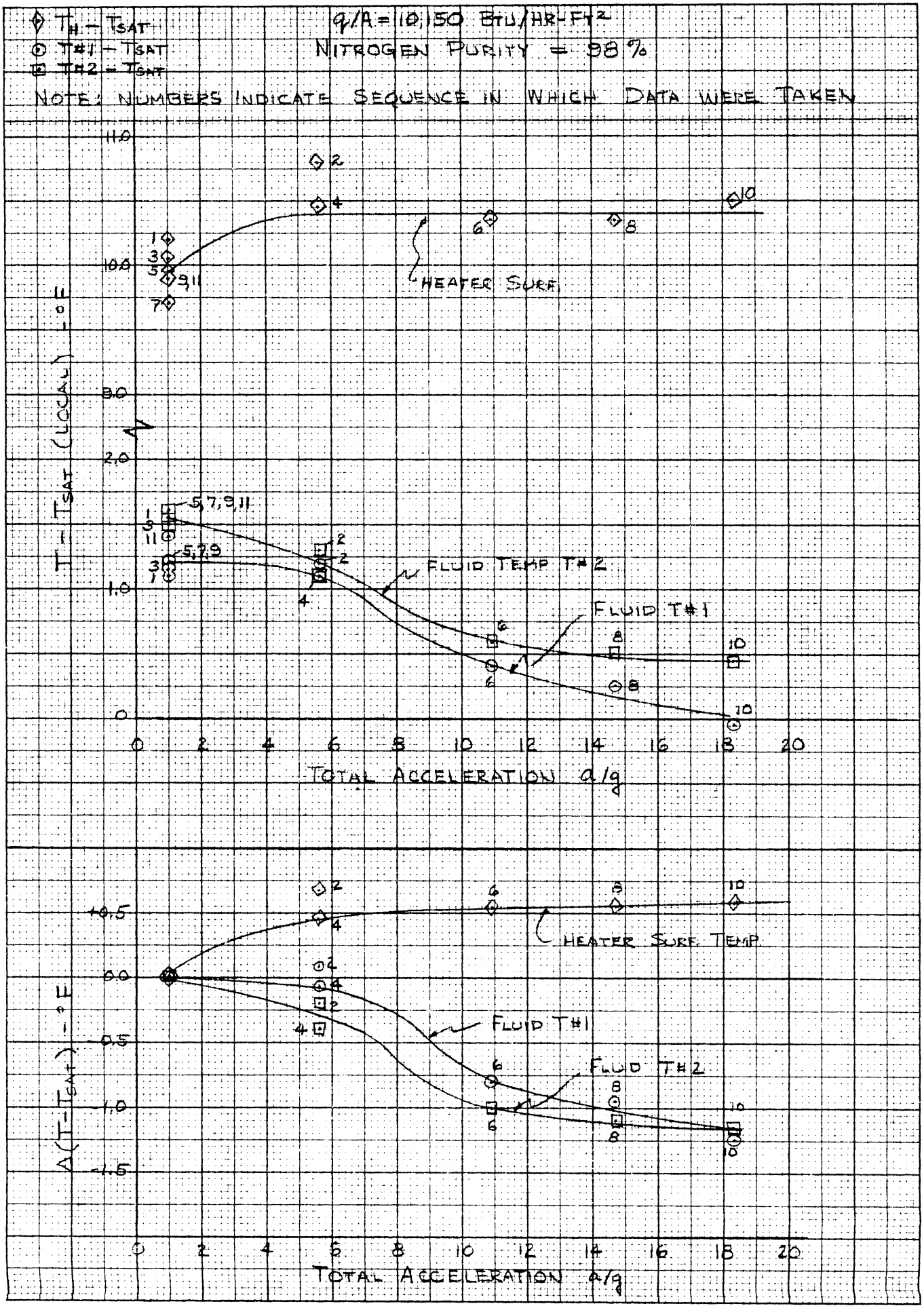

FIGURE 33. COMPOSITE PLOT FOR LIQUID DEPTH OF 2.5 INCHES
RUN NO. 21

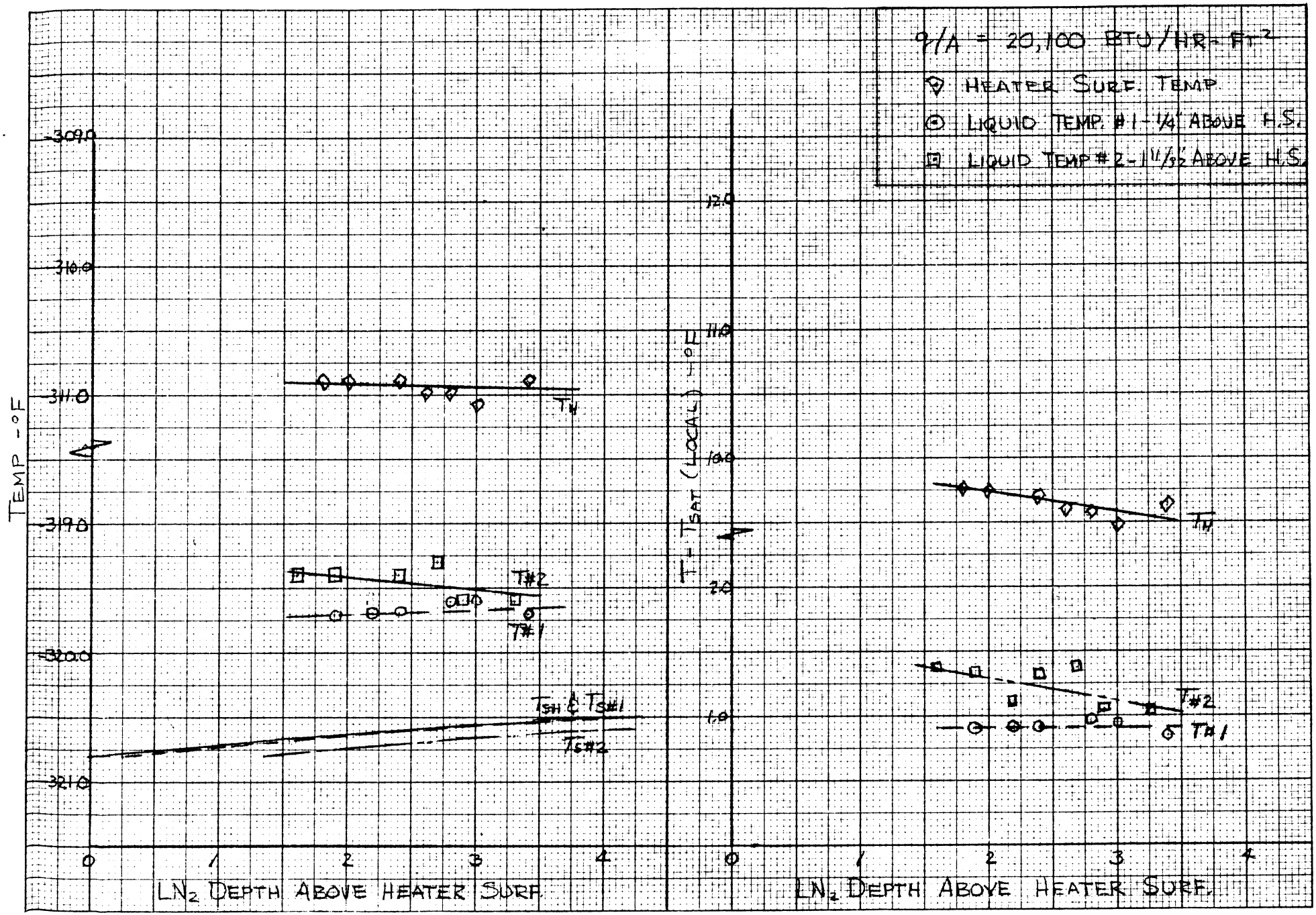

FIGURE 35. INFLUENCE OF LIQUID DEPTH ON TEMPERATURES
RUN NO. 22 a/g = 2.6

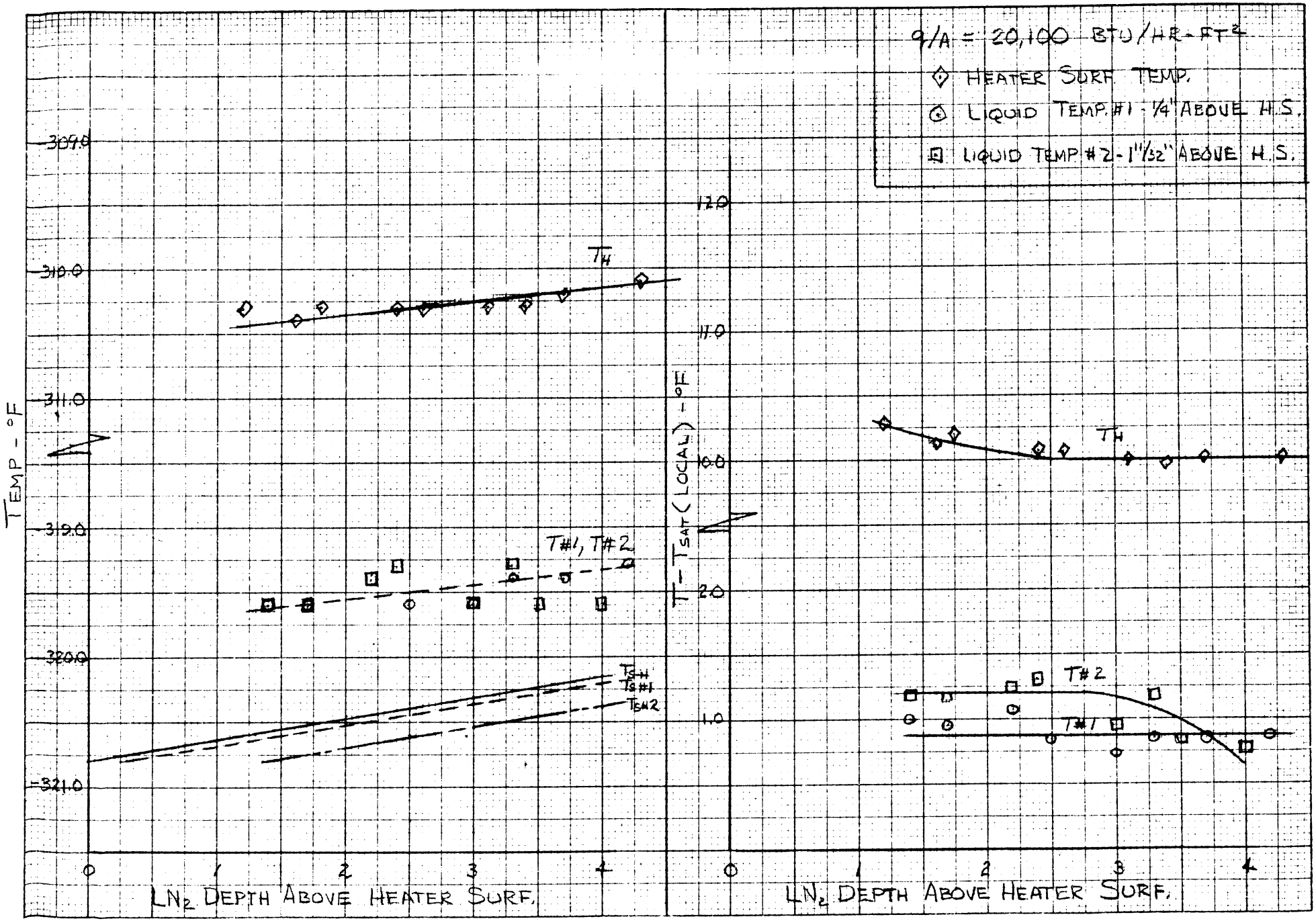

FIGURE 36. INFLUENCE OF LIQ. DEPTH ON TEMPERATURES
RUN NO. 22 $a/g = 5.6$

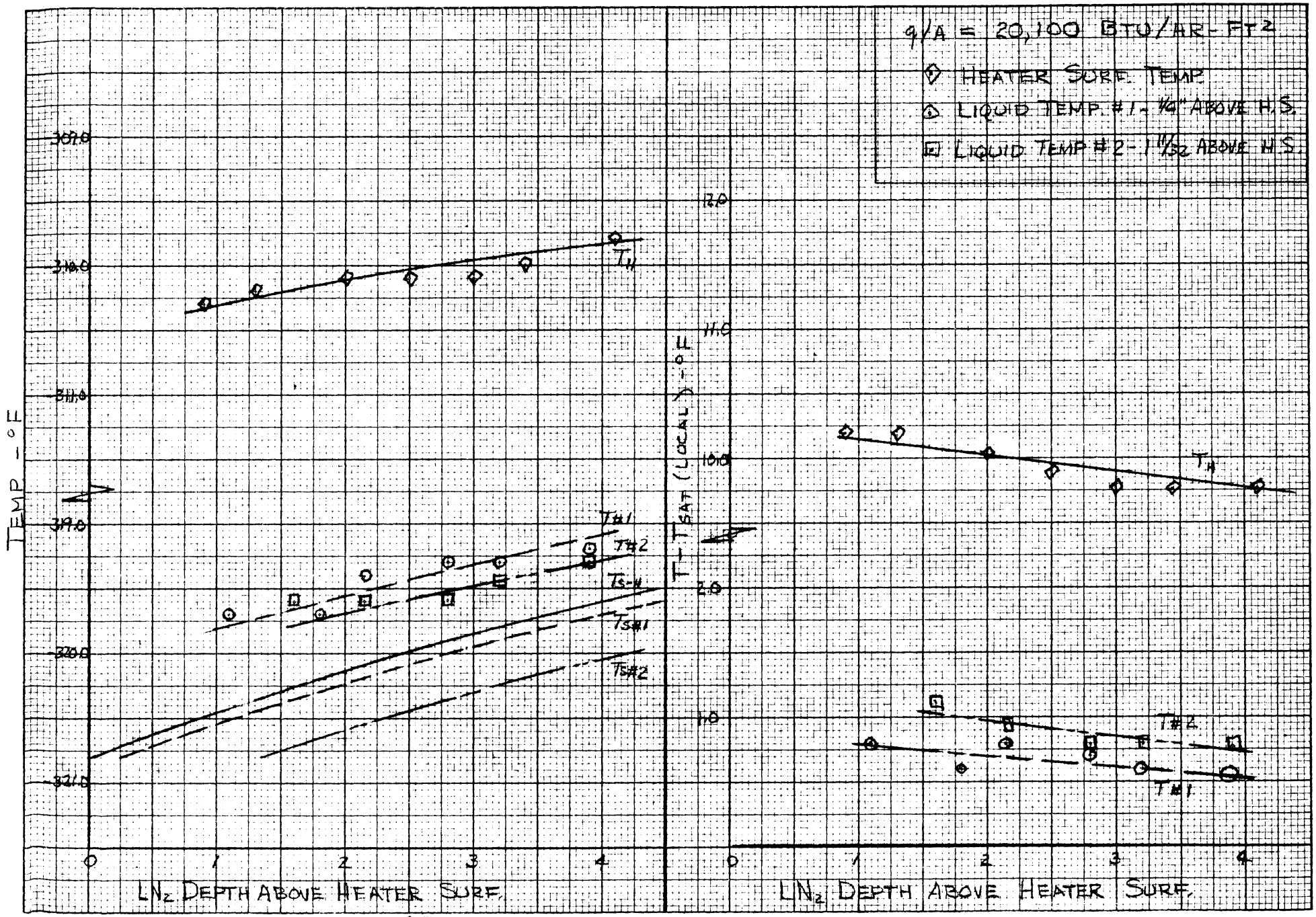

FIGURE 37 . INFLUENCE OF LIQUID DEPTH ON TEMPERATURES
RUN NO. 22 $a/g = 10.9$

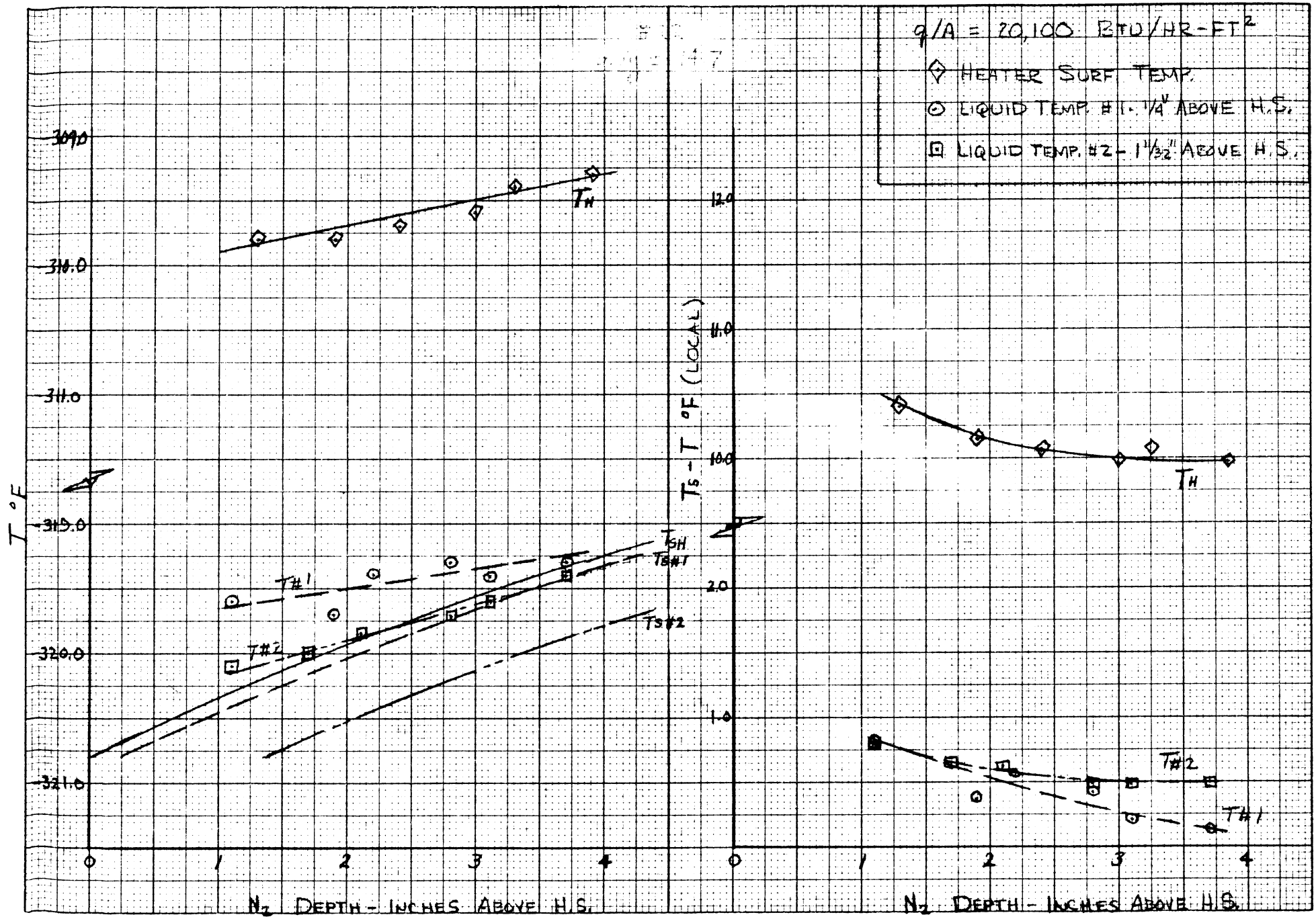

FIGURE 38. INFLUENCE OF LIQUID DEPTHS ON TEMPERATURES
RUN NO. 22 $a/g = 14.7$

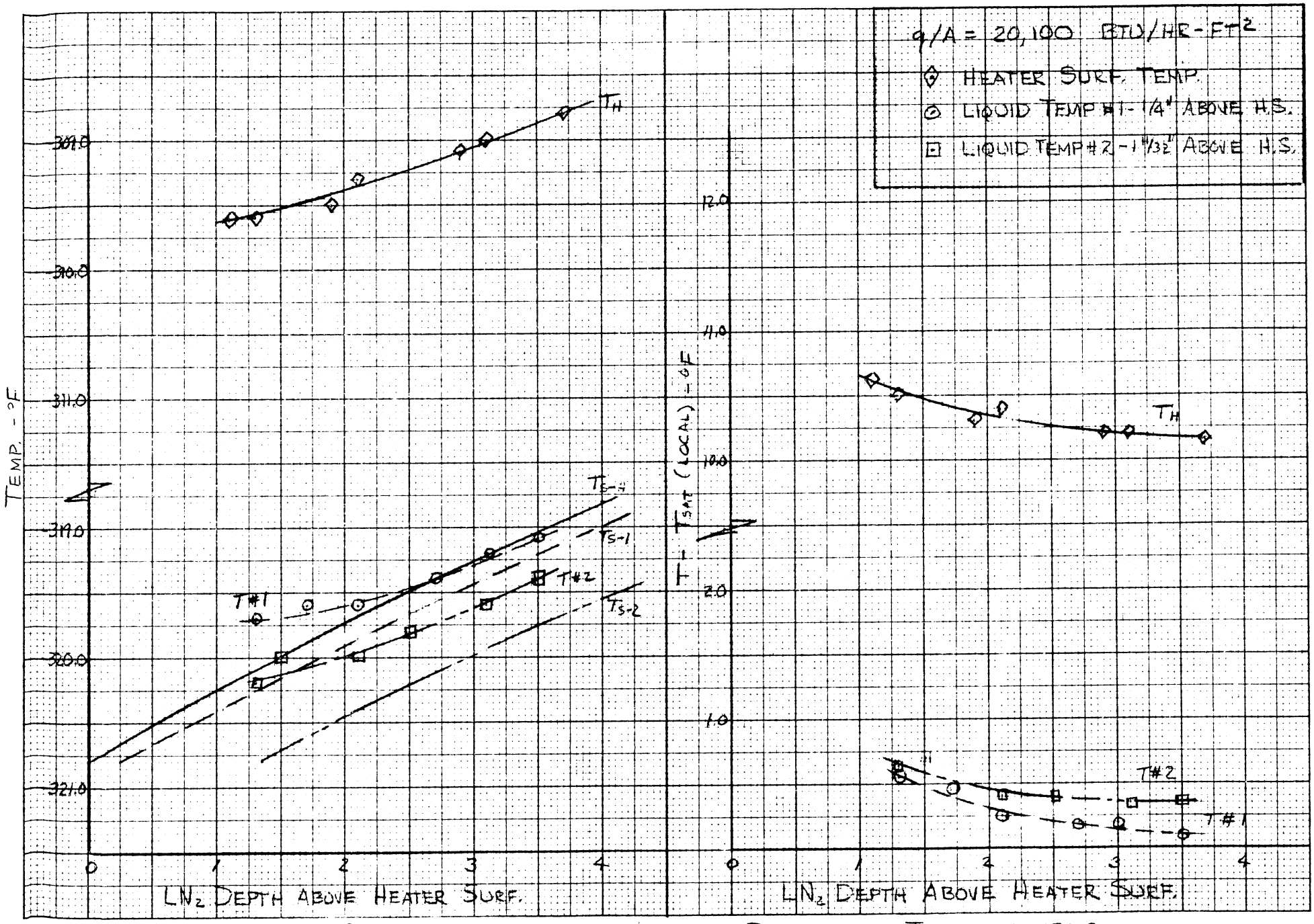

FIGURE 39. INFLUENCE OF LIQUID DEPTH ON TEMPERATURES
RUN NO. 22 $q/q = 18.3$

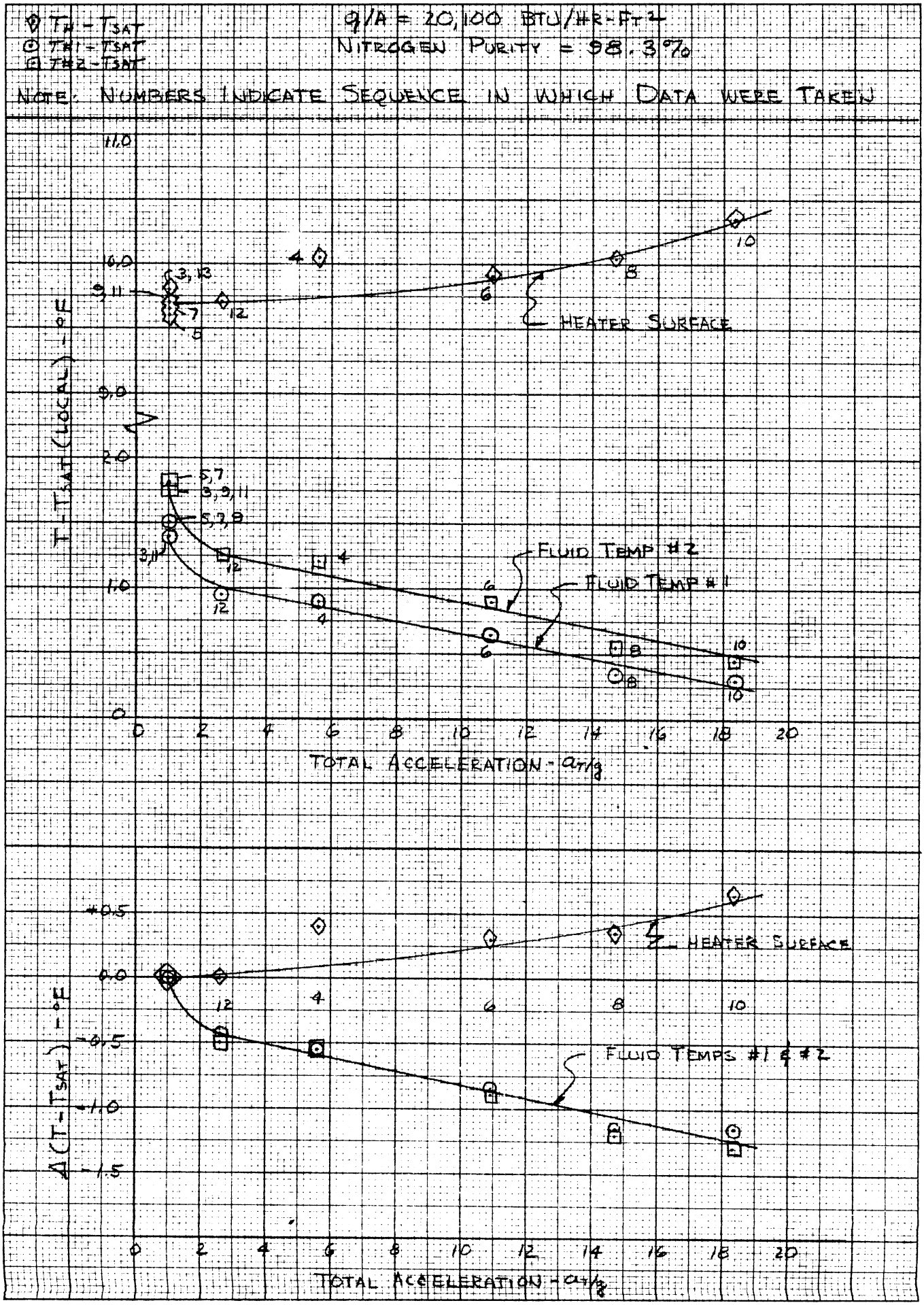

FIGURE 40. COMPOSITE PLOT FOR LIQUID DEPTH OF 2.5 INCHES
RUN NO. 22

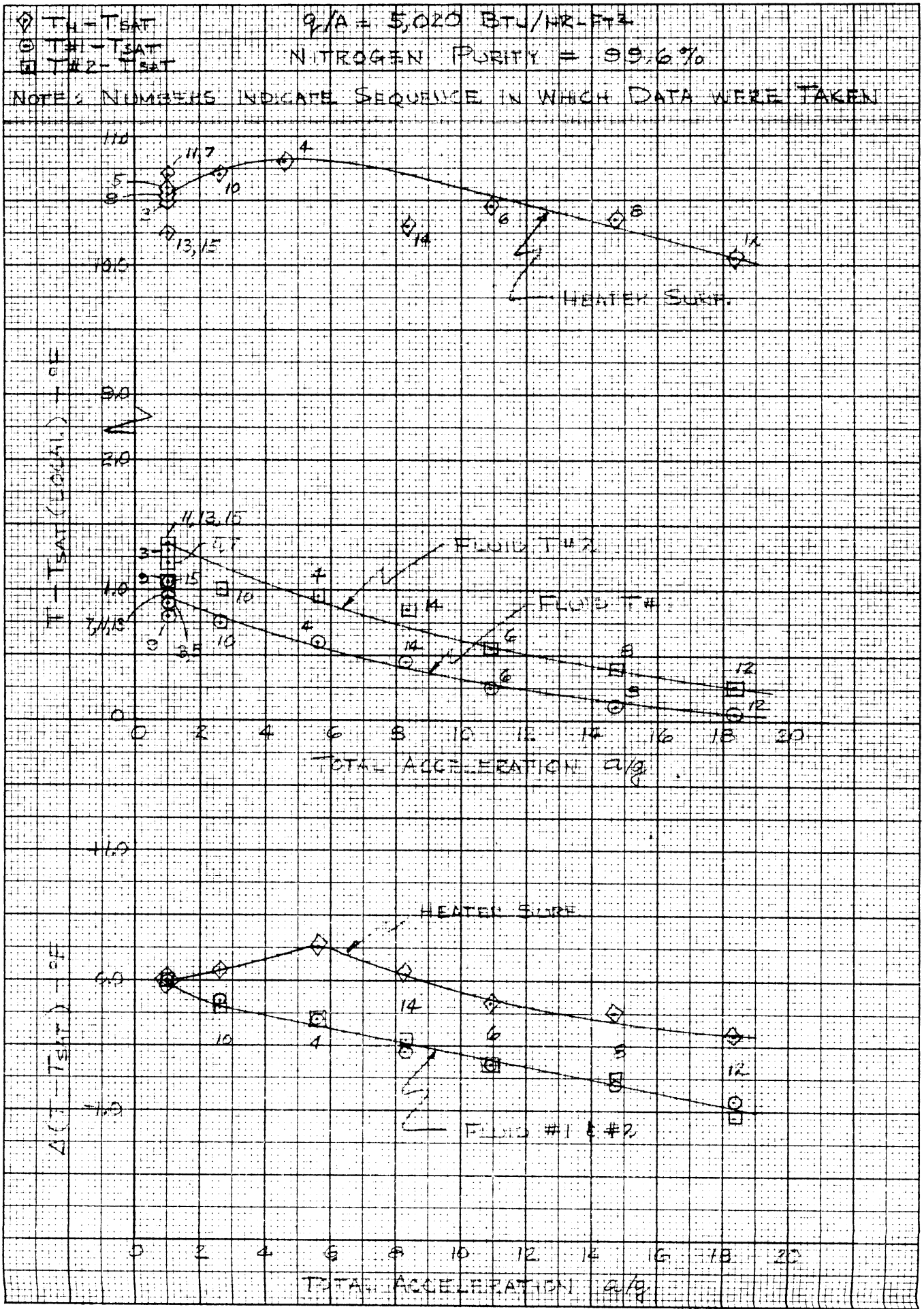

FIGURE 42. COMPOSITE PLOT FOR LIQUID DEPTH OF 2.5 INCHES
RUN NO. R2

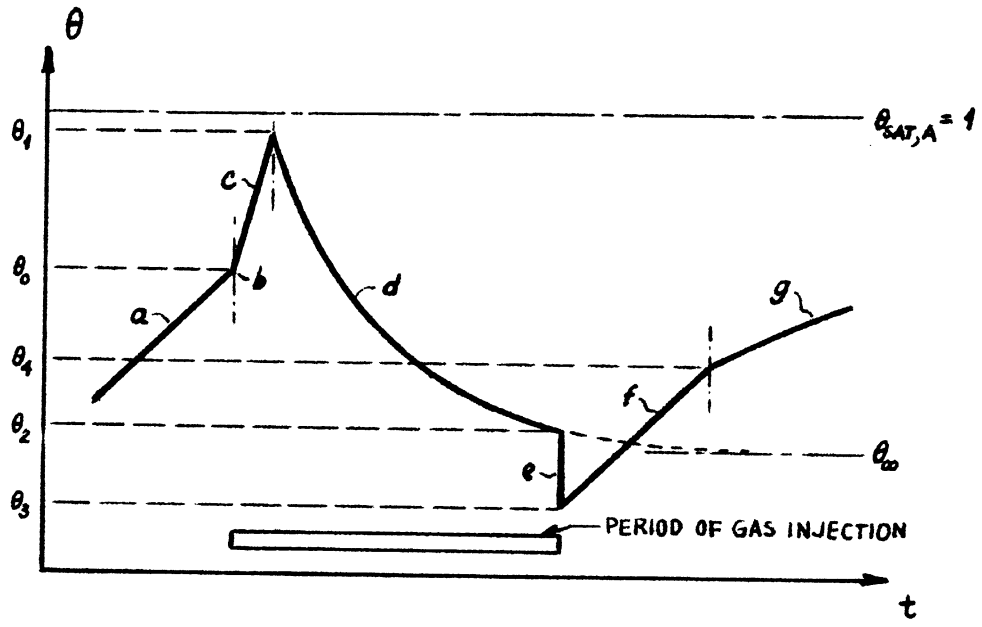

a. ambient heating

b. liquid displacement transient

c. gas injection with liquid phase present only

d. gas injection with two-phase equilibrium

e. liquid back-flow from reservoir. Mixing

f. ambient heating of subcooled two-component mixture

g. ambient heating of saturated two-component mixture

Fig. 43: General lumped system temperature transient in response to ambient heating and a period of injection of a highly soluble gas. - Schematic.

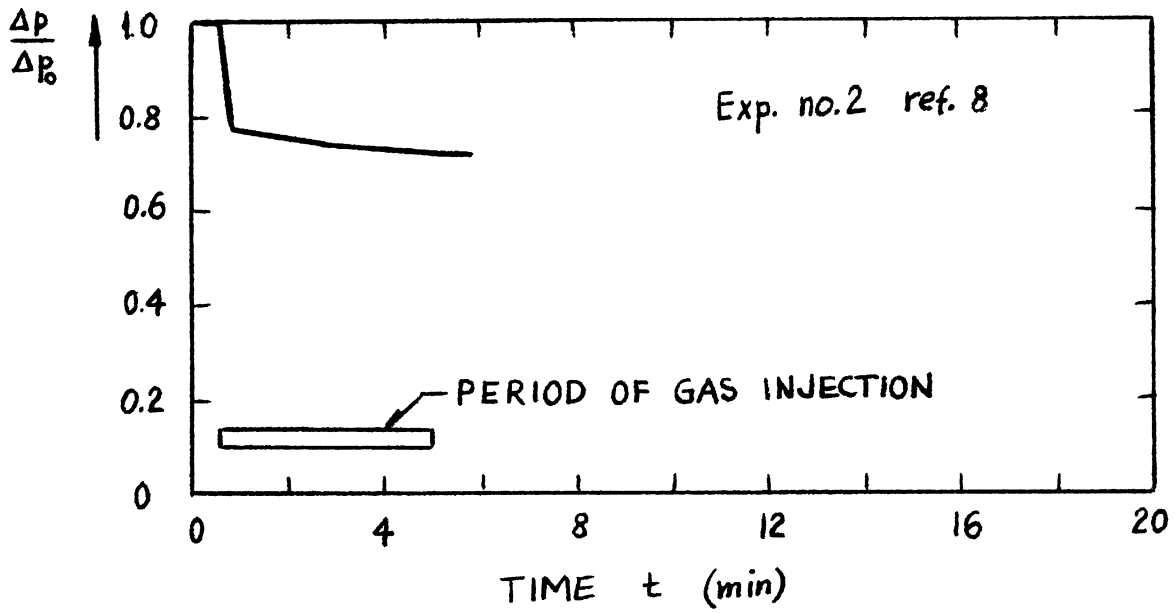

FIG. 44 - DIFFERENTIAL PRESSURE OVER FIXED COLUMN LENGTH

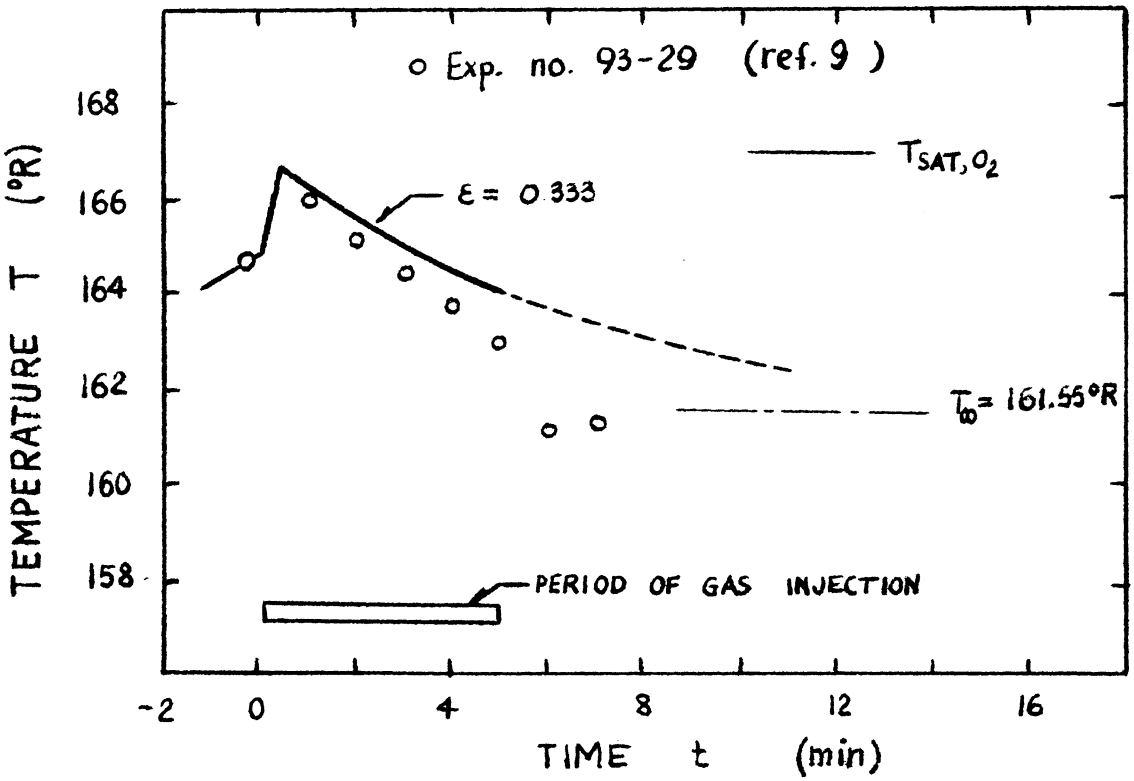

FIG. 45 - LIQUID OXYGEN COOLED BY NITROGEN INJECTION

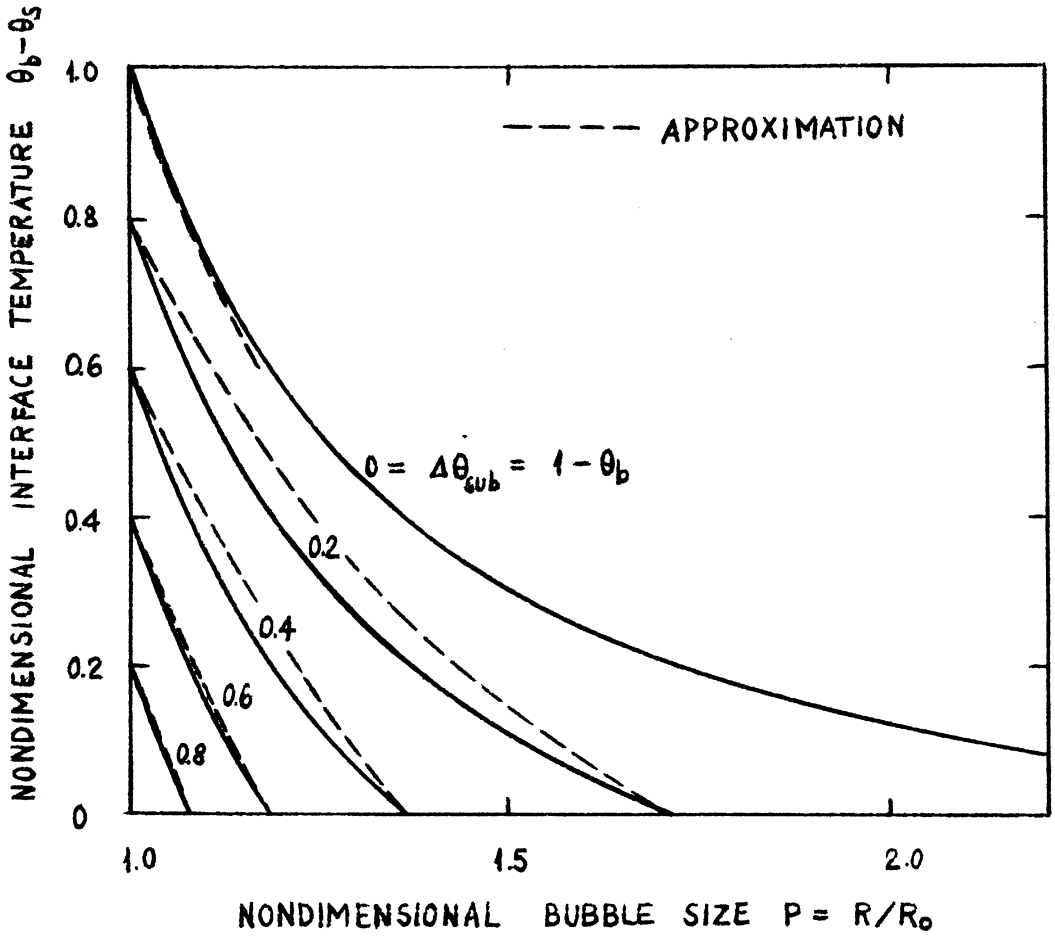

FIG. 46 - INTERFACE TEMPERATURE vs. BUBBLE SIZE - BULK LIQUID SUBCOOLING $\Delta\theta_{sub}$ PARAMETER - LUMPED GAS PHASE

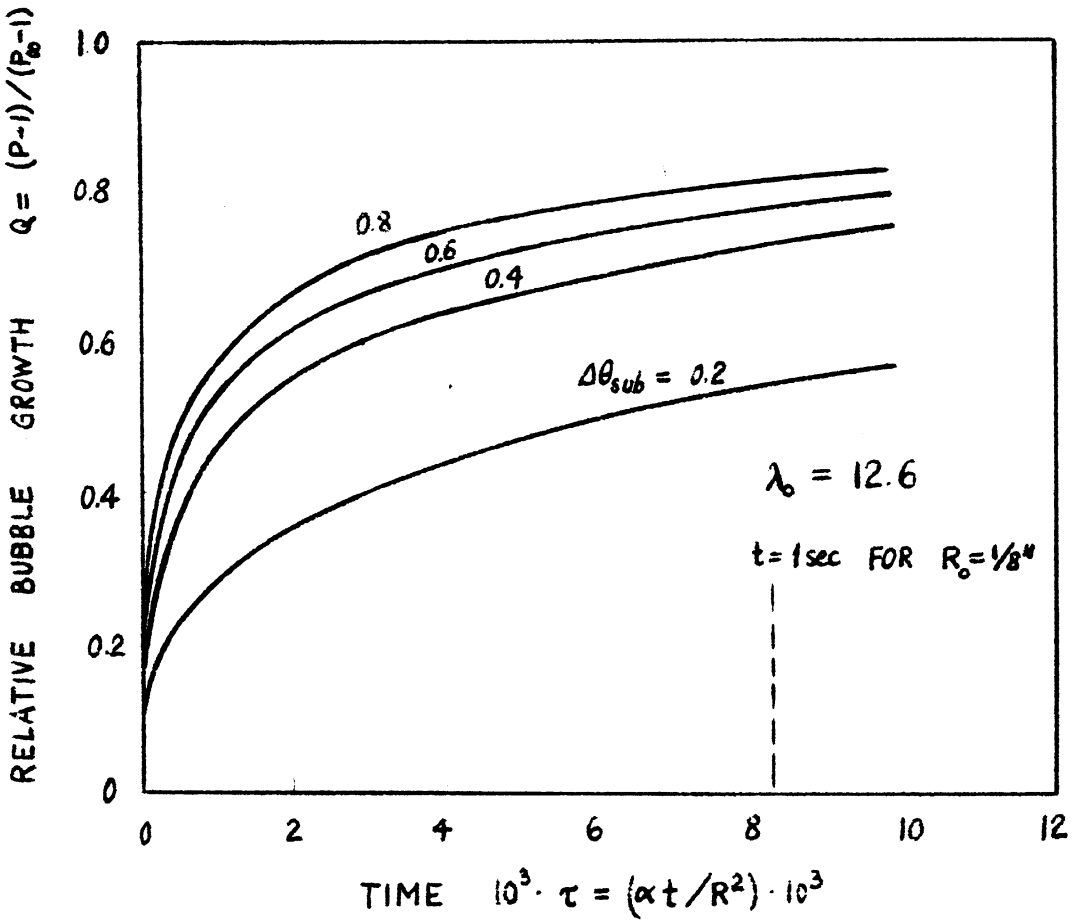

FIG. 47 – RELATIVE NONDIMENSIONAL BUBBLE GROWTH – LIQUID OXYGEN 184°R 3.1 atm.

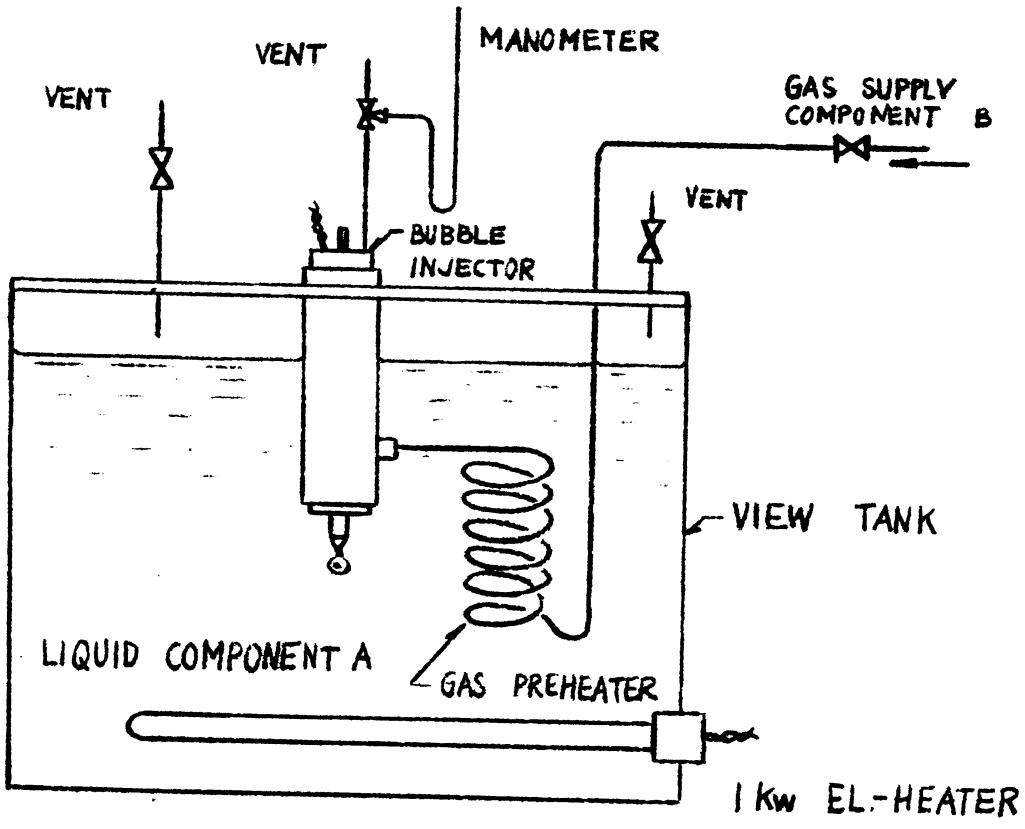

FIG. 48 - EXPERIMENTAL SET-UP FOR STUDY OF THE DYNAMICS OF SINGLE STATIONARY BUBBLES

UNIVERSITY OF MICHIGAN
3 9015 02827 4218